**Khalil Al Handawi**
Mechanical Engineering,
McGill University,
Montreal H3A 0C3, Canada
e-mail: khalil.alhandawi@mail.mcgill.ca

**Petter Andersson**
Multidisciplinary Design Optimization,
GKN Aerospace Engine Systems,
Trollhättan 46138, Sweden
e-mail: petter.andersson@gknaerospace.com

**Massimo Panarotto**
Industrial and Materials Science,
Chalmers University of Technology,
Göteborg 41296, Sweden
e-mail: massimo.panarotto@chalmers.se

**Ola Isaksson**
Professor
Industrial and Materials Science,
Chalmers University of Technology,
Göteborg 41296, Sweden
e-mail: ola.isaksson@chalmers.se

**Michael Kokkolaras**[1]
Associate Professor
Mechanical Engineering,
McGill University,
Montreal H3A 0C3, Canada
e-mail: michael.kokkolaras@mcgill.ca

# Scalable Set-Based Design Optimization and Remanufacturing for Meeting Changing Requirements

*Design requirements are often uncertain in the early stages of product development. Set-based design is a paradigm for exploring, and keeping under consideration, several alternatives so that commitment to a single design can be delayed until requirements are settled. In addition, requirements may change over the lifetime of a component or a system. Novel manufacturing technologies may enable designs to be remanufactured to meet changed requirements. By considering this capability during the set-based design optimization process, solutions can be scaled to meet evolving requirements and customer specifications even after commitment. Such an ability can also support a circular economy paradigm based on the return of used or discarded components and systems to working condition. We propose a set-based design methodology to obtain scalable optimal solutions that can satisfy changing requirements through remanufacturing. We first use design optimization and surrogate modeling to obtain parametric optimal designs. This set of parametric optimal designs is then reduced to scalable optimal designs by observing a set of transition rules for the manufacturing process used (additive or subtractive). The methodology is demonstrated by means of a structural aeroengine component that is remanufactured by direct energy deposition of a stiffener to meet higher loading requirements.*
[DOI: 10.1115/1.4047908]

*Keywords: design flexibility, design for remanufacturing, additive manufacturing, set-based design, design optimization*

## 1 Introduction

The increasing environmental impact of industrial activities is changing the perception of legislators and business enterprises toward the importance of a circular economy (CE) for achieving both economic growth and environmental protection. Since resources are limited, legislation has been put forth so that business enterprises bear responsibility for the environmental, social, and economic impacts their products have on society [1]. This caused business enterprises to adopt sustainable development practices when designing their products.

A closed-loop supply chain (CLSC) can return used or discarded products to working condition. This enables sustainable development by reducing the environmental impact of products [2]. A CLSC includes a forward supply chain where products are used normally until the end of their life and a reverse supply chain that returns the discarded products to a previous stage in its lifecycle. Examples of recovery activities in a reverse supply chain include remanufacturing, reuse, and recycling [3,4]. Since CE encompasses products as well as their forward and reverse supply chains, businesses must design their products for closed-loop product recovery activities [3]. This includes design for remanufacturing, recycling, and reuse. There is a number of studies that consider product design for remanufacturing [5,6]. However, the majority focus on closed-loop supply chain logistics of remanufacturing [7–11].

Design requirements are subject to change during a product's lifecycle [12–15]. Variable parameters such as customer requirements and loading conditions influence design requirements such as cost and product life requirements [16] and can be unpredictable despite the best efforts of forecasters and analysts [17]. Product development methods must thus incorporate design *changeability*, whose aspects can include flexibility, agility, robustness, and adaptability. A number of basic and extended principles have been identified as enablers of design changeability [16].

Arguably, a set of flexible solutions is required to leverage the added design changeability in order to provide possible alternative designs. Set-based design (SBD) is a design paradigm that places emphasis on a varied solution set as a means for accommodating uncertain requirements. Feasibility of the solutions with respect to the requirements and changeability must be checked and maintained throughout the solution set.

In this paper, we propose a design optimization methodology that provides a set of solutions to accommodate changing requirements through remanufacturing. We focus on remanufacturing since it is more sustainable than recycling and recovers more value across the supply chain due to increased virgin material substitution and retention of the embodied energy used to manufacture the original product from the raw materials [4,12].

The paper is organized as follows. Section 2 reviews theoretical background and the literature. Section 3 outlines the proposed methodology, which is then applied to a structural aeroengine component to be remanufactured by additive manufacturing (AM) deposition to meet higher loading requirements. Section 4 introduces the case study, formulates the corresponding design problem, and discusses results. Section 5 provides concluding remarks and identifies possible future research directions.

## 2 Background

In this section, we review the literature in the following areas to contextualize our contribution to design for remanufacturing:

- Product design for remanufacturing.
- Design changeability and flexibility assessment.

[1]Corresponding author.

Contributed by the Design Automation Committee of ASME for publication in the Journal of Mechanical Design. Manuscript received March 4, 2020; final manuscript received June 22, 2020; published online August 18, 2020. Assoc. Editor: Eun Suk Suh.

  

- Set-based design (SBD) approaches.

**2.1 Product Design for Remanufacturing.** Additive manufacturing (AM) presents potential economic and environmental benefits. While this work considers component remanufacturing in general, we focus on the use of AM to realize its potential benefits. Remanufacturing by AM has been characterized as an enabler of a circular economy due to its ability to repair damaged components and thus avoid the production of new components [18]. Lifecycle cost savings up to 50% are reported for remanufacturing by AM of a stamping tool as well as turbine blades [19]. However, to realize the environmental benefits of this new technology, the build process of the part must also be optimized and embedded within the product design problem [20]. Design for remanufacturing rules found in the literature specify that a product's components should allow room for modifications to meet design requirements [20]. Furthermore, it is important to distinguish refurbishment from remanufacturing: the former is used to satisfy original specifications, whereas the latter allows for considering changed requirements.

The effectiveness of AM for remanufacturing end-of-life (EoL) components is reported in Refs. [9,21]. They consider replacement strategies and EoL decisions regarding reuse, recycling, or remanufacturing. However, there are some notable studies that have introduced remanufacturing considerations into component design. Level set topology optimization was used in Ref. [6] to optimize a structural component considering subtractive remanufacturing. A containment constraint is formulated and used to ensure that a remanufactured design is contained within the material domain of the parent design. This methodology yields designs that can be scaled down by remanufacturing. However, it does not consider the reverse operation of remanufacturing by additive methods. Furthermore, variable loading requirements are not considered.

Environmental impact was considered an optimization objective for a topology optimization problem of a structural component in Ref. [22]. Additive manufacturing was accommodated by incorporating life cycle analysis (LCA) considerations into the design problem. Although this is not a remanufacturing study, the ability of AM to enable remanufacturing is underlined.

An important feature of a product's lifecycle is upgrade, defined as an improvement at the specifications level [23]. The upgrade levels for remanufacturing of a product are usually predetermined and are not adjusted based on required specifications at the end-of-life. Based on this, a strategy for determining the optimal market position in terms of pricing and remanufacturing costs can be developed [24]. This study addresses the major activities of remanufacturing which include product takeback (the process of collecting end-of-life products for the activity of remanufacturing, modeled using several scenarios where the remanufacturer either passively accepts all end-of-life products or selectively purchases them), remanufacturing operations, and remarketing. Decisions are then made regarding the reusability of the end-of-life product's components. The target specifications for components in need of an upgrade is optimized to maximize revenue from resale of the remanufactured product. The upgrade levels for remanufacturing are captured using generational differences defined as the amount of discrepancy between the current component's specifications and those of components in recent cutting edge products.

It can be thus argued that successful remanufacturing requires a product's components to be designed for such activities to maximize environmental benefits. The main principle governing the ease of upgrading component specifications involves design changeability defined as the property of a system to undergo specified classes of changes with relative ease and efficiency [25]. As a result, a review of flexible design practices is warranted.

**2.2 Quantifying Changeability in Product Design.** A product and its operating environment undergo change during design and operation in order to stay relevant in dynamic markets. Change events are characterized by three elements: (i) the agent of change, (ii) the mechanism of change, and (iii) the effect of change.

The change agent is the instigator for change in the product and is specified in the form of product requirements. The nature of the change agent helps identify the type of change the system must undergo. If the change is external to the product system (e.g., environmental operational conditions) then the change is of a *flexible* type. If the change agent is internal to the system (e.g., sizing and tolerance requirements) then it is of an *adaptable* type.

The change effect is the difference between the states of a product before and after the change. Based on the nature of change effects, three more changeability aspects are defined. *Robustness* is defined as the insensitivity of the design to internal or external change (e.g., stability of a vehicle despite changes in road conditions and grade). *Scalability* is the ability of the design to change to meet a different level of a specification (e.g., reinforce a structural member to carry a larger load than originally intended). *Modifiability* is the ability of the design to change in order to accommodate unforeseen requirements not native to the original design (e.g., ability of a cargo plane to be repurposed for reconnaissance missions) [26]. This term is also referred to as *evolvability* in the literature [27].

A system may undergo some or all types of change. Several works in the literature have attempted to quantify and capture the changeability of a product system for embedding this principle in product design. Tackett et al. use the product system's capability of meeting design requirements to quantify the available excess capacity for evolving [27]. Based on the excess available in a product, an evolvability metric based on the principle of stored elastic energy in a system is computed. The evolvability metric is a relative metric that is useful for comparative design studies.

Other studies focus on quantifying flexibility as a result of predictable and unpredictable changes in the operating environment [28,29]. In one study, the tradeoff between various requirements (referred to as design objectives and performances) is captured by a Pareto set. Movement along the shortest path from one end of the Pareto set to the other is penalized by a change cost. Flexible designs are identified as a ranged set between the extremes of the Pareto set such that the overall change costs are minimized [28].

The notion of flexible ranged sets is also investigated by other researchers [29]. Candidate target sets of solutions that maximize a flexibility metric over the set are identified in the design space by mapping flexible designs identified in the requirements space. The design and requirements spaces are defined as the set of possible values the design variables or requirements can assume, respectively. The process begins by producing a number of design alternatives through probing the design space. The design alternatives are mapped on the requirements space (referred to as the attribute space). Design alternatives are partitioned into ranged sets in the requirements space. A flexibility metric for each set is calculated by integration of an influence function over the set. Sets that maximize flexibility are preferred as possible design solutions.

Suh et al. considered *modularity* of product platforms as a means for achieving changeability [25]. Requirement bandwidths (referred to as product attributes) are computed based on the market conditions for the product platform. Optimization is used to position product platforms in the market (similar to Ref. [24]) and compute design bandwidths. Monte Carlo simulation is used to evaluate the effect of uncertainty in the market on the net present value of the product platform. The sensitivity of flexible and inflexible product platforms to uncertainty is compared. In this study, only predetermined product variants are considered as part of the product platform. As explained earlier, in a remanufacturing context, it is important to adjust the upgrade levels of the product based on changes in the requirements [24].

Flexibility can be considered in both the design space and requirements space [30]. When reviewing the available literature, it appears that quantifying changeability is performed largely in the requirements space rather than the design space and a methodology for mapping between the two spaces is required to identify the most flexible designs [27–29,31]. Furthermore, when considering

changeability due to changes in the operating environment and the product, it is important to consider a set of solutions that are changeable in order leverage the added flexibility of the design solutions [25,28,29]. A single point design that is flexible would not be justified if no alternatives are offered. Finally, among the mentioned aspects of changeability, scalability appears to be of most relevance to remanufacturing since it involves upgrading the specifications of a product's components to achieve the required change. As a result, we will focus on set-based design principles while considering a metric for identifying scalable solution sets for remanufacturing purposes.

**2.3 Set-Based Design Principles and Applications.** Due to the high level of uncertainty at the early phases of the product development process, designers have adopted iterative product design methods. Traditionally, the design problem is solved by selecting an initial design based on existing knowledge or expert opinion as an initial "seed" in the design space. The initial seed design is improved iteratively until a satisfactory design that meets the design requirements is reached. This paradigm is known as point-based design (PBD) [32–34]. PBD allows the design engineers to arrive at a solution in a short time frame. However, once the design engineers commit to a solution in the design phase, it becomes difficult to modify the design should the system requirements change during the later stages of the product development process [35,36].

A possible remedy to the above shortcomings is to delay commitment to a single design early in the design stage. SBD is another design paradigm that addresses this by exploring alternative designs in the early stages of product development and delay commitment to a single design. The set of alternative designs is developed simultaneously until the variable parameters driving the requirements have been refined. Only the set of designs that has been refined by the updated requirements is developed further. This results in several designs rather than a single design that are gradually refined over the course of the product development process.

Sobek et al. [34] identify three principles to be observed during SBD. (1) The design space is explored to identify feasible designs comprising the feasible design set (FDS) with respect to each design requirement and quantify trade-offs between possible design solutions. (2) The intersection of the FDSs is identified in (1) while still maintaining flexibility in the offered design solutions. (3) The FDS is gradually narrowed down by eliminating undesirable solutions as design requirements become more well-defined and constraints are tightened. It can be concluded that a SBD methodology should feature (i) design maps of the FDSs that are transferable to ease communication between different engineering teams, (ii) must capture arbitrarily shaped FDSs, (iii) assess feasibility of design solutions efficiently to offset the longer lead time associated with SBD, and (iv) have the ability to incorporate designer preferences as a means for eliminating designs.

There are several works that address the SBD principles introduced in Ref. [34] quantitatively. They can be classified into works that focus on either design feasibility assessment or design space reduction based on performance and designer preferences.

Interval arithmetic has been used to map the FDS [32,37]. Qureshi et al. [32] partition the design space into hyper-rectangle domains in which feasibility is assessed. If feasibility is not established throughout the hyper-rectangle, the domain is further subdivided and feasibility is checked in each subdivision until all feasible hyper-rectangles are identified. *Noise* variables associated with uncertain parameters in the set-based context are quantified by means of intervals. Hyper-rectangles that lie within noise variable intervals are considered a subset of the robust design space. The method is intuitive and effective at reducing the design space to a manageable subspace. However, design spaces cannot always be captured by hyper-rectangles due to their irregular shapes. This is because uncertain parameters and design variables may affect several requirements simultaneously. This often causes the feasible regions that satisfy the requirements to assume highly irregular shapes including disconnected regions. Moreover, design requirements are often not given as analytic expressions of the design variables and parameters but are obtained from simulation models. Fuzzy set theory has been used to accommodate design variable uncertainties in the context of SBD [38]. However, fuzzy sets describe the membership of a quantity over an interval or a hyper-rectangle just like classical sets which may be inadequate for capturing arbitrarily shaped design spaces. The SBD approach is similar to the notion of ranged sets described earlier [29].

Convex hulls have been used to identify the feasible sets while design constraints have been used to treat design requirements [39]. The constraints are perturbed to represent variability of the design requirements, resampling in proximity of the constraint is used to refine the convex hull and redefine the FDS. The method can capture irregularly shaped design spaces and is intuitive. However, this methodology is computationally intensive due to the need for constant resampling as the design problem evolves (especially if expensive engineering models are used to calculate the constraints).

Another feasibility assessment tool is formulated using Bayesian network classifiers (BNCs) [40–42]. The motivation of this work comes from using constraint programming (CP) to identify feasible solution sets [31]. CP requires analytical expressions of the system constraints to map the feasible regions. As mentioned above, such analytical expressions are not always available in simulation-based design problems. In these cases, metamodels can be used as surrogates of the constraint functions. BNCs use a set of training data generated by engineering models to train a kernel density estimate (KDE) for estimating a posterior probability distribution for feasible and infeasible design events. The decision surface is computed from the intersection of the two probability distributions and a threshold probability (typically 0.5) is used to render feasibility decisions [40]. The method is systematic and can accommodate a constant stream of data from the designer. Furthermore, the BNC approach can render decision boundaries for irregularly shaped design spaces and produce a KDE that can be communicated with other design teams for visualizing the feasible set of each subsystem in question. Finally, Monte Carlo simulation can be used to calculate the volume of the reduced design space for comparative studies [31].

SBD principles have also been extended to platform development [25,43] and conceptual design [44]. Platform assessment processes have been used to ensure feasibility of the narrowed-down set-based solutions in platform development of product variants. The process blocks are integrated in a product lifecycle management (PLM) architecture to facilitate information exchange between the platform assessment blocks [43]. Wang and Terpenny [44] employ a design synthesis technique to generate concepts using an agent-based modeling approach to conceptual design. The generated concepts embody the FDS for conceptual design.

So far, the studies reviewed provide means for identifying set-based solutions. SBD principles involve narrowing down the FDS to a handful of acceptable designs for further investigation and detailed design. Several works have presented a design or concept elimination methodology for narrowing down feasible sets by eliminating undesirable designs in terms of performance or designer preferences.

A diversity metric can be used to develop a representative cost for configurations within the FDS of the design space associated with the risk of violating feasibility [45]. Malak et al. [46] use utility theory to make set-based decisions. Interval dominance criterion was used to eliminate designs when there is no overlap in their uncertainty ranges. The maximality criterion was used to make decisions involving design variables with overlapping uncertainty intervals. Nahm and Ishikawa [37] accommodate designer preferences in the form of "preference numbers" and functions. The designer's preference structure spans design variables and requirements which may be a product of multidisciplinary analyses. However, as with fuzzy sets, the approach may not span arbitrarily shaped design spaces.

In most design problems, a number of competing objectives or attributes often arise. This is the case with SBD problems. Wang and Terpenny [44] used a genetic algorithm to evaluate alternative design trade-offs in a component-based system synthesis problem. A generalized weighted aggregate of fuzzy-set preferences was used as an optimization objective. Avigad and Moshaiov [47] solved a trade-off problem based on the optimality and variability (OAV) of each conceptual design in the design space. The two metrics are extracted from the Pareto sets associated with each set-based concept [47]. Trade-off rules are subjective to designer preferences and are a good approach for accommodating designer preferences during design elimination.

Miller et al. [48] investigated a multi-fidelity approach to SBD, where increasing levels of fidelity are concurrently met with increasing level of detail in the set-based solutions. The refinement is carried out over a modeling sequence to minimize the cost associated with modeling effort. Interval dominance is used to gradually narrow down the solution set for each model used.

Hannapel and Vlahopoulos [49] present a multidisciplinary design optimization (MDO) approach to set-based design by treating the design space boundaries as design variables for the system-level optimization problem. The discipline problems are solved individually for a specific objective and are coordinated by the system-level optimization problem. The objective of the system-level problem is an aggregate of design space hypervolume, weighted sum of individual discipline objectives and relaxable constraint violation. By solving the MDO problem, the design space is narrowed down. Design performance is accommodated in the discipline-level optimization problems. The methodology assumed a design space in the form of a hyper-rectangle as prescribed by the design variable intervals. However, practical engineering design problems feature irregularly shaped design spaces [40]. Furthermore, the utilized weighted method assumes a convex attainable set for the objectives considered in the system-level optimization problem, which is not necessarily the case [50].

We classify the SBD methods based on the set-based representation of the obtained design solutions. The two distinct representations that emerge are ranged sets [25,28,29,32,37] and response surfaces [31,39,40,51]. Response surfaces have the advantage of being able to capture irregularly shaped design spaces and are more conservative in comparison to hyper-rectangular sets. Shahan and Seepersad [40] and Yannou et al. [31] accommodate nonlinear design requirements through various metamodels such as BNCs and polynomial response surfaces (PRSs) used as surrogates of feasibility models.

SBD methods consider predominantly computational design engineering problems. However, the surrogate models used by Shahan and Seepersad [40] and Yannou et al. [31] can be used with experimental, testing, and operational data from the component being remanufactured. This makes surrogate models useful for a wide range of engineering design problems.

Finally, a number of techniques for narrowing down the set-based solution has been proposed. These techniques include Pareto set membership [28,48], optimality of a ranged set with respect to an objective function (design performance or flexibility) [25,29,49], and interval dominance for ranged sets [46,48].

**2.4 Proposed Approach.** Our objective is to generate a set of changeable component designs that can be upgraded as necessary through remanufacturing to meet changing requirements that may arise at a product or system's end-of-life.

We propose a systematic design space reduction methodology using optimization and response surfaces. An optimization problem is formulated to include parameters reflecting requirements. We then obtain a set of parametric optimal solutions to maximize the performance of the remanufactured products. Since designers must commit to a solution eventually, it is important to consider the changeability of a product throughout its lifecycle and not just at the design stage to allow products to retain most of their economic value [16]. We therefore incorporate a scalability constraint in our SBD methodology to further reduce our solutions set to readily changeable designs. The scalability constraint is evaluated in the requirements space since changeability and scalability by proxy are defined in the requirements space. The set of possible parameter values related to performance requirements are used as a proxy of the requirements space. We provide a mapping between the design space and the parameter space to map scalable designs identified in the parameter space back to the design space. The proposed methodology is based on

- surrogates of the computational models for rapid evaluations during optimization,
- numerical optimization for identifying the best performing feasible designs as for different design parameter values, i.e., a set of *parametric* optimal designs,
- response surfaces of the parametric optimal design solutions that provide a mapping of design solutions between the design and parameter spaces,
- sensitivity analysis of design variables with respect to design parameters,
- a remanufacturing constraint based on the sensitivity of design variables to design parameters and manufacturing process capabilities that reduces the set of parametric optimal designs to a set of *scalable* optimal designs in the parameter space.

The proposed methodology, presented as a flow diagram in Fig. 1, is presented in detail in Sec. 3.

## 3 Methodology

Engineering design optimization problems involve decision variables $\mathbf{x} \in \mathbb{R}^n$ and design parameters $\mathbf{p} \in \mathbb{R}^m$. Objective ($f(\mathbf{x}; \mathbf{p})$) and constraint ($\mathbf{g}(\mathbf{x}; \mathbf{p})$) functions are used to reflect design requirements. Given bounded design optimization variables and parameters $\mathbf{L} \le \mathbf{x} \le \mathbf{U}$ and $\mathbf{L}_p \le \mathbf{p} \le \mathbf{U}_p$, respectively, we define the design space $D$ and the parameter space $P$. We also consider constraint sets $C_u$ for $u = 1, 2, \ldots, q$ where $q$ is the number of constraints. In a product design context, constraints are part of the design requirements and are driven by the parameters $\mathbf{p}$. Finally, the feasible set $F$ is defined as the intersection of all constraint sets and contains designs that meet all design requirements. The set $F$ is the FDS and represents the outcome of SBD before elimination of potential designs.

Design parameters may affect the optimal solution of the optimization problem due to their influence on design requirements. As a result, designs that are optimal throughout the parameter space $P$ and satisfy the design requirements comprise the set of parametric optimal designs which is a reduction of the FDS. Since practical SBD methodologies require solutions sets that can be easily communicated across design teams, response surfaces are used as a surrogate model to evaluate feasibility and performance and to classify membership of each design to the feasible set and the set of parametric optimal designs.

**3.1 Surrogate Modeling.** The objective and constraint functions used to represent design requirements are evaluated using computer-aided engineering (CAE) tools that model the repair/remanufacturing process. These computational models are computationally expensive. Any SBD methodology requires a large number of function evaluations to investigate not only the design but also the parameter space. Therefore, we resort to building less expensive response surfaces to be used as surrogate models.

Ge et al. [51] introduced a surrogate-based SBD methodology to facilitate interactive negotiations in design engineering groups who are responsible for design tasks at different hierarchical levels, i.e., at the system, subsystem, and component levels. Surrogate models are used to capture the interactions and the dynamics of the engineering systems and subsystems and are used to map feasible design regions (FDRs) and effective design regions (EDRs) to satisfy design requirements and performances respectively.

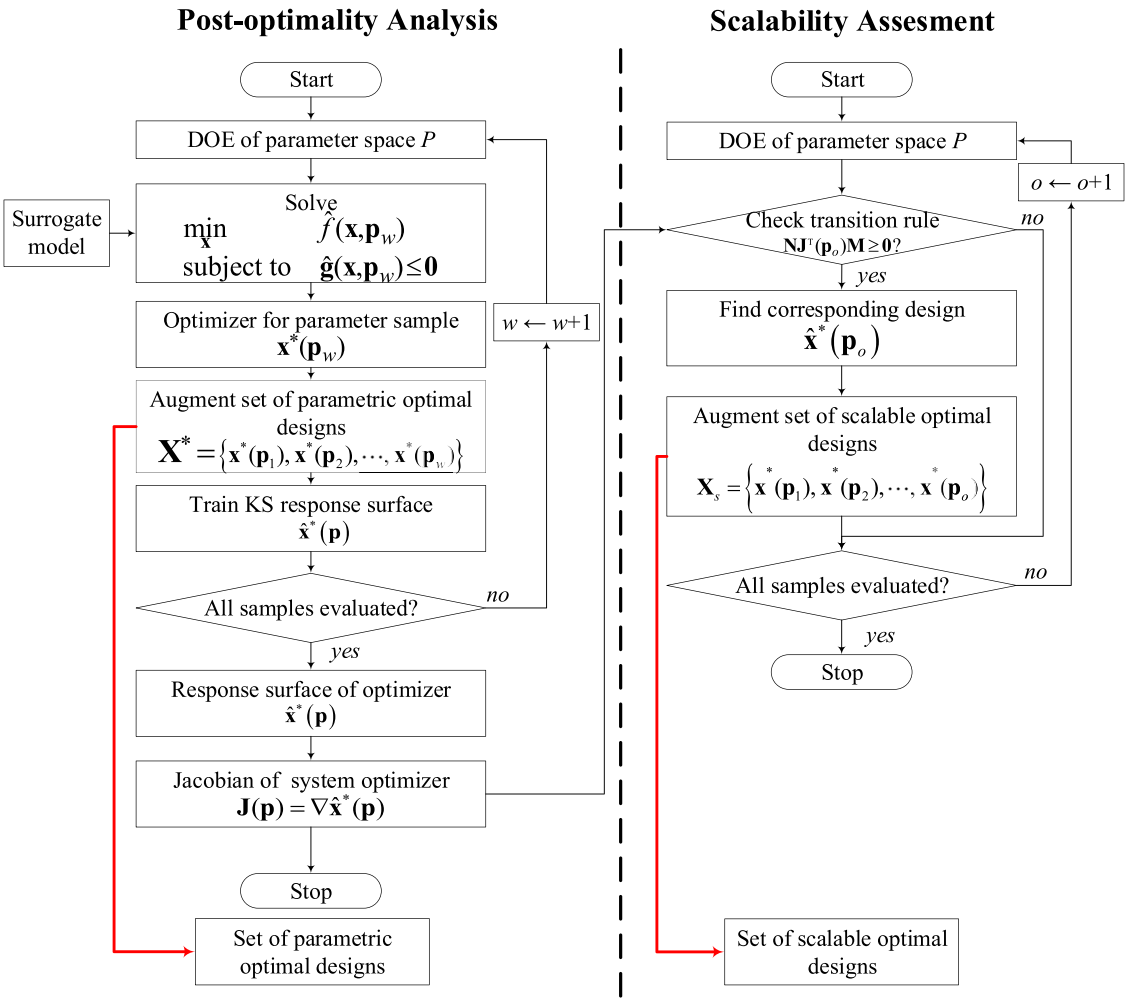


**Fig. 1 Set-based design space reduction methodology**

Finally, robustness is evaluated using the hypervolume of the EDRs as a metric. The larger the hypervolume, the more robust is the EDR [52].

We conduct designs of experiments to sample the aggregate design and parameter spaces and then exercise the computational models at these sample points to generate adequate training data. An ensemble of surrogate models is then constructed and denoted by $\hat{f}(\mathbf{x};\mathbf{p})$ and $\hat{\mathbf{g}}(\mathbf{x};\mathbf{p})$. An open source surrogate model library is used to build the surrogates [53,54].

An order-based metric is used to assess the predictive capability of the surrogates [55]. This metric ensures the consistency between the computationally expensive and surrogate model predictions. The order-based metric is also used for constructing response surfaces of the parametric optimal solutions with respect to varying design parameters in subsequent sections and is discussed using a numerical example in Sec. 3.4.

**3.2 Parametric Optimal Designs.** We use numerical optimization to provide a set of design solutions that can address a range of requirements. Specifically, we solve the optimization problem for different parameter values. This can be seen as a form of post-optimality analysis (POA) that provides the sensitivity of optimal design variable values with respect to varying parameter values [56].

The surrogate optimization problem is formulated as

$$\begin{aligned} \underset{\mathbf{x}}{\text{minimize}} \quad & \hat{f}(\mathbf{x};\mathbf{p}) \\ \text{subject to} \quad & \hat{\mathbf{g}}(\mathbf{x};\mathbf{p}) \le \mathbf{0} \end{aligned} \tag{1}$$

and solved to obtain the solution $\mathbf{x}^*(\mathbf{p})$. Given intervals for the parameters $\mathbf{p}$, sampling techniques can be used to obtain a set of $m$ combinations. Here, we use Latin hypercube (LH) sampling that produces a uniform random distribution over the parameter space [57]

$$\mathbf{P} = \begin{bmatrix} \mathbf{p}_1^{\mathrm{T}} \\ \mathbf{p}_2^{\mathrm{T}} \\ \vdots \\ \mathbf{p}_w^{\mathrm{T}} \end{bmatrix} = \begin{bmatrix} p_{11} & p_{12} & \cdots & p_{1m} \\ p_{21} & p_{22} & \cdots & p_{2m} \\ \vdots & \vdots & \ddots & \vdots \\ p_{w1} & p_{w2} & \cdots & p_{wm} \end{bmatrix} \tag{2}$$

LH sampling is used since the number of samples needed to fit an adequate response surface scales better with dimensionality relative to uniform sampling techniques such as full factorial sampling. Once we have obtained a solution $\mathbf{x}^*(\mathbf{p})$ for each of the $w$ parameter vectors, a response surface $\hat{\mathbf{x}}^*(\mathbf{p})$ is built using the set of parametric optimal designs $\mathbf{X}^* = \{\mathbf{x}^*(\mathbf{p}_1), \mathbf{x}^*(\mathbf{p}_2), \ldots, \mathbf{x}^*(\mathbf{p}_w)\}$. A rule of thumb indicates that the initial sample size should be about an order of magnitude larger than the dimensionality of the problem, i.e., $w \approx 10\,m$) [58]. To potentially save computational cost, we also monitor the convergence rate of the order-based error as more samples are added and accept the response surface as adequate

once it has reached an appropriate threshold. An example of this procedure is provided in Sec. 3.4. The response surface $\hat{\mathbf{x}}^*(\mathbf{p})$ is used to predict parametric optimal designs throughout the parameter space.

Sensitivity gradients of the design variables with respect to the parameters allow designers to understand the effect of requirement changes to optimal designs. The Jacobian of $\hat{\mathbf{x}}^*(\mathbf{p})$ is

$$\mathbf{J}(\mathbf{p}) = \nabla\hat{\mathbf{x}}^*(\mathbf{p}) = \begin{bmatrix} \nabla\hat{x}_1^{*\mathrm{T}}(\mathbf{p}) \\ \nabla\hat{x}_2^{*\mathrm{T}}(\mathbf{p}) \\ \vdots \\ \nabla\hat{x}_n^{*\mathrm{T}}(\mathbf{p}) \end{bmatrix} = \begin{bmatrix} \frac{\partial\hat{x}_1^*}{\partial p_1} & \frac{\partial\hat{x}_1^*}{\partial p_2} & \cdots & \frac{\partial\hat{x}_1^*}{\partial p_m} \\ \frac{\partial\hat{x}_2^*}{\partial p_1} & \frac{\partial\hat{x}_2^*}{\partial p_2} & \cdots & \frac{\partial\hat{x}_2^*}{\partial p_m} \\ \vdots & \vdots & \ddots & \vdots \\ \frac{\partial\hat{x}_n^*}{\partial p_1} & \frac{\partial\hat{x}_n^*}{\partial p_2} & \cdots & \frac{\partial\hat{x}_n^*}{\partial p_m} \end{bmatrix} \tag{3}$$

It can be estimated using the derivatives of the basis functions used to construct the response surface. Differentiation of the response surface is possible because it is based on a linear combination of basis functions. We use a Kernel Smoothing (KS) model to build $\hat{\mathbf{x}}^*(\mathbf{p})$ and estimate the Jacobian $\mathbf{J}(\mathbf{p})$ using the linear combination of the gradient of the kernel functions. KS was used to construct the response surface due to their immediate computation since it does not require matrix inversions. Furthermore, KS models typically respect the order of the output which reflects its ability to predict the correct order of values of any two evaluation points. This is very important for this application since it relies on differentiating the KS model [55].

For the remainder of this subsection, let us use the typical notation between an independent variable $x$ and a dependent variable $y$ recalling however, that in our context $\hat{\mathbf{x}}^*(\mathbf{p})$ is corresponding to $y$ (dependent variable) while $\mathbf{p}$ is corresponding to $x$ (independent variable). KS models consist of a weighted sum of training points where the weight for each training point decreases as the distance from the prediction point increases:

$$\begin{aligned} \hat{y}(\mathbf{x}) &= \frac{\sum_{j=1}^{w}\phi_j(\mathbf{x})y_j}{\sum_{j=1}^{k}\phi_j(\mathbf{x})} \\ &= \frac{\phi_1(\mathbf{x})y_1 + \phi_2(\mathbf{x})y_2 + \cdots + \phi_w(\mathbf{x})y_w}{\phi_1(\mathbf{x}) + \phi_2(\mathbf{x}) + \cdots + \phi_w(\mathbf{x})} \\ &= \frac{\phi_1(\mathbf{x})y_1}{\phi_1(\mathbf{x}) + \phi_2(\mathbf{x}) + \cdots + \phi_w(\mathbf{x})} + \frac{\phi_2(\mathbf{x})y_2}{\phi_1(\mathbf{x}) + \phi_2(\mathbf{x}) + \cdots + \phi_w(\mathbf{x})} \\ &\quad + \cdots + \frac{\phi_w(\mathbf{x})y_w}{\phi_1(\mathbf{x}) + \phi_2(\mathbf{x}) + \cdots + \phi_w(\mathbf{x})} \end{aligned} \tag{4}$$

where $\phi_j$ is the kernel function for the $j$th training point, $y_j$ is the output at the $j$th training point, and $\mathbf{x}$ is the prediction point. To determine the gradient of $\hat{y}(\mathbf{x})$, the quotient rule of differentiation is applied to each term in Eq. (4), and the common terms are factored out to yield

$$\begin{aligned} \nabla\hat{y}(\mathbf{x}) &= \frac{\phi_1(\mathbf{x}) + \phi_2(\mathbf{x}) + \cdots + \phi_w(\mathbf{x})}{\left[\phi_1(\mathbf{x}) + \phi_2(\mathbf{x}) + \cdots + \phi_w(\mathbf{x})\right]^2} \\ &\quad \times \left[\nabla\phi_1(\mathbf{x})y_1 + \nabla\phi_2(\mathbf{x})y_2 + \cdots + \nabla\phi_w(\mathbf{x})y_w\right] \\ &\quad - \frac{\nabla\phi_1(\mathbf{x}) + \nabla\phi_2(\mathbf{x}) + \cdots + \nabla\phi_w(\mathbf{x})}{\left[\phi_1(\mathbf{x}) + \phi_2(\mathbf{x}) + \cdots + \phi_w(\mathbf{x})\right]^2} \\ &\quad \times \left[\phi_1(\mathbf{x})y_1 + \phi_2(\mathbf{x})y_2 + \cdots + \phi_w(\mathbf{x})y_w\right] \\ &= \frac{\sum_{j=1}^{w}\phi_j(\mathbf{x})\sum_{j=1}^{w}\nabla\phi_j(\mathbf{x})y_j - \sum_{j=1}^{w}\nabla\phi_j(\mathbf{x})\sum_{j=1}^{w}\phi_j(\mathbf{x})y_j}{\left[\sum_{j=1}^{w}\phi_j(\mathbf{x})\right]^2}. \end{aligned} \tag{5}$$

We used the Gaussian kernel function (and its gradient) defined as

$$\phi_j(\mathbf{x}) = e^{-\pi\lambda\|\mathbf{x}-\mathbf{x}_j\|_2} \tag{6}$$

$$\nabla\phi_j(\mathbf{x}) = -\frac{\pi\lambda(\mathbf{x}-\mathbf{x}_j)}{\|\mathbf{x}-\mathbf{x}_j\|_2}e^{-\pi\lambda\|\mathbf{x}-\mathbf{x}_j\|_2} \tag{7}$$

where $\lambda$ is the bandwidth of the kernel function. The bandwidth parameter's effect on the order-based error is also used to determine the optimal bandwidth for adequately capturing the Jacobian of the KS model. Equations (6) and (7) are substituted into Eq. (5) to provide the gradient of the prediction function $\hat{y}(\mathbf{x})$. This process is repeated for each of the design variables $\hat{x}_1^*(\mathbf{p}), \hat{x}_2^*(\mathbf{p}), \ldots \hat{x}_n^*(\mathbf{p})$ to populate the Jacobian in Eq. (3).

**3.3 Reduction to Set of Scalable Optimal Designs.** We adopt the terminology used by Ross et al. [26] for defining the aspects of design changeability. Varying design parameters as proxies of requirements is a *change agent* that provides motivation for changing the design. *Scalability* represents the ability of the design to adapt to changing requirements by means of scaling. For example, a design that is in service must now sustain a higher static load than originally intended during the design phase. This change can be accommodated by reinforcing the structure using AM techniques. Transition rules may govern changes. For example, the reinforcement can only add material to the design and not subtract from it (analogous to the containment rule formulated by Liu and Ma [6] for subtractive remanufacturing). Furthermore, there is a cost and time associated with the change. As a result, designs that minimize the transition costs while maximizing the offered alternatives should be considered during SBD to add more value to the design. We focus here on *transition rules* that consider the ability of the manufacturing process to scale the design.

We derive transition rules pertaining to additive and subtractive manufacturing. AM processes can only add material to the substrate that results in an increase in the volume of the deposit. The opposite applies to subtractive manufacturing. The volume of the deposited part must be described in terms of the design variables pertaining to the geometry. The monotonicity of the volume with respect to each design variable is the basis for selecting designs that are scalable. For example, a variable such as the thickness of a beam has a positive monotonicity with respect to the beam volume. This is because an increase in the beam thickness leads to an increase in beam volume. Conversely, a variable such as hole diameter through the thickness of the beam has a negative monotonicity with respect to the beam volume. This is because a larger hole will subtract more material from the volume of the beam.

In this work, we focus on variables where a strict monotonic increase or decrease with respect to volume can be determined. Variables that do not have a monotonic impact on volume are excluded from the analysis. We consider a problem involving four design variables denoted as $x_1$, $x_2$, $x_3$ and $x_4$. Equation (8)

$$V = f(x_2^+, x_3^+) \tag{8}$$

reflects the fact that only variables $x_2$ and $x_3$ have a monotonic impact on volume, where the superscripts + and − denote increasing and decreasing monotonicity, respectively. We define a monotonicity vector $\mathbf{m}$ of $n$ components; $m_l = 1$ if the monotonicity of the volume with respect to variable $x_l$ is increasing and $m_l = -1$ if the monotonicity is decreasing, where $l = 1, 2, \ldots, n$. Opposite signs for $m_l$ should be used if subtractive manufacturing is considered. If the designer wishes to neglect the effect of variable $x_l$ on the volume, then $m_l = 0$. For example, based on Eq. (8), $\mathbf{m} = [0\ 1\ 1\ 0]^{\mathrm{T}}$. A diagonal matrix $\mathbf{M}$ is then constructed as

$$\mathbf{M} = \begin{bmatrix} 0 & 0 & 0 & 0 \\ 0 & 1 & 0 & 0 \\ 0 & 0 & 1 & 0 \\ 0 & 0 & 0 & 0 \end{bmatrix} \tag{9}$$

Similarly, a vector characterizing the change agent $\mathbf{n}$ can be defined for the system parameters $\mathbf{p}$ to describe the sign of the change: $n_i = 1$ if parameter $p_i$ is expected to increase and $n_i = -1$ if the parameter is

expected to decrease, where $i = 1, 2, \ldots, m$. If, for example, the vector $\mathbf{n}$ is defined as $\mathbf{n} = [1 -1 -1]^T$ a diagonal matrix $\mathbf{N}$

$$\mathbf{N} = \begin{bmatrix} 1 & 0 & 0 \\ 0 & -1 & 0 \\ 0 & 0 & -1 \end{bmatrix} \tag{10}$$

is constructed similar to above.

In order to select designs that are scalable, the required change in the variable must result in either an increase or no change in volume. This is expressed in Eq. (11).

$$n_i m_l \frac{\partial \hat{x}_l^*}{\partial p_i} \geq 0 \tag{11}$$

The non-strict inequality includes zero-valued components to accommodate nonsensitive variables where $m_l = 0$. The transition rule can be formulated in matrix form as

$$\mathbf{N}\mathbf{J}^T(\mathbf{p})\mathbf{M} \geq \mathbf{0} \tag{12}$$

Every element of the resulting matrix must be greater than or equal to zero in order to satisfy the transition rule.

To illustrate Eq. (12), a two-dimensional parameter space example is shown in Fig. 2.

The change agent vector $\mathbf{n}$ describes a quadrant (or hyper-octant in higher dimensions) in the parameter space that should contain the gradient vector $\nabla\hat{\mathbf{x}}^*(\mathbf{p})$. The sign of the gradient vector is modified by the monotonicity vector $\mathbf{m}$. Figure 2 shows an example when $m_l \nabla \hat{x}_1{}^*(\mathbf{p}) \geq 0$ and lies within the quadrant defined by $\mathbf{n}$. Designs within the change agent quadrant and having gradients leading to an increase in their value are considered scalable.

In order to map scalable designs from the parameter space to the design space, the design space is resampled randomly and the transition rule (Eq. (12)) is checked for every sample $\mathbf{p}_o$. If $\mathbf{N}\,\mathbf{J}^T(\mathbf{p}_o)\mathbf{M} \geq \mathbf{0}$ is satisfied then the corresponding design $\hat{\mathbf{x}}^*(\mathbf{p}_o)$ is retrieved and appended to a set of scalable solutions $\mathbf{X}_s$.

**3.4 Numerical Example for Determining the Scalable Design Set.** We demonstrate the concepts related to constructing a KS response surface to estimate the Jacobian using a numerical example. We also show how the estimated Jacobian can be used for identifying the scalable design set. Himmelblau's test function is used as it features multiple local minima. The test function and its Jacobian are

$$x^*(p_1, p_2) = ({p_1}^2 + p_2 - 11)^2 + (p_1 + {p_2}^2 - 7)^2$$

and

$$\mathbf{J}(p_1, p_2) = \begin{bmatrix} 4p_1({p_1}^2 + p_2 - 11) + 2(p_1 + {p_2}^2 - 7) \\ 2({p_1}^2 + p_2 - 11) + 4p_2(p_1 + {p_2}^2 - 7) \end{bmatrix},$$

respectively.

We approximate the response surface for this function via KS to obtain $\hat{x}^*(\mathbf{p})$. For this example, we set the change agent vector as $\mathbf{n} = [1 -1]$ and the monotonicity vector as $\mathbf{m} = [1]$. The test function is sampled via Latin hypercubes to create the training data for the KS model. We evaluate the transition rule $\mathbf{N}\,\mathbf{J}^T(\mathbf{p})\mathbf{M} \geq \mathbf{0}$ defining the scalable set using the analytical and estimated Jacobian. The estimated Jacobian was obtained by differentiation of the KS basis functions. A portion of the Latin hypercube samples are reserved for use as a validation set and are not used to train the KS model. The cross-validation error reflects the accurately of the KS response surface at the validation points as part of the true scalable set obtained from the analytical Jacobian.

In addition, we use the order-based error proposed in Ref. [55] since it does not rely on comparisons with the true scalable set (which is not available in real problems). It is computed by checking how accurately the response surface model orders the validation points. It is calculated as

$$\varepsilon_{OE} = \frac{1}{n_{cv}^2} \sum_{i=1}^{n_{cv}} \sum_{l=1}^{n_{cv}} \theta\left(\mathbf{x}^*(\mathbf{p}_i) - \mathbf{x}^*(\mathbf{p}_l), \hat{\mathbf{x}}^*(\mathbf{p}_i) - \hat{\mathbf{x}}^*(\mathbf{p}_l)\right) \tag{13}$$

where $n_{cv}$ is the number of validation points. The function $\theta$ is defined as

$$\theta(a,b) = (a \leq 0) \text{ xor } (b \leq 0) \tag{14}$$

where xor is the logical *exclusive or* operator. Figure 3 shows the effect of the number of training points ($n_{samples}$) and the bandwidth ($\lambda$) on the cross validation and order-based errors.

It can be seen that there is a unique combination of $n_{samples}$ and $\lambda$ that yield the best response surface for assessing scalability in the parameter space. The true and estimated scalable sets are shown in Fig. 4. The KS model used for the estimation is trained using 2305 training samples and a bandwidth of $\lambda = 0.054$. Figure 4 shows that KS is capable of capturing the scalable set despite underestimating the magnitude of the test function. Figure 3 shows that the order-based error is a good indication of the prediction accuracy of the KS model for the scalable set. As a result, the KS parameters and number of training points can be determined by minimizing the order-based error.

In summary, the proposed methodology consists of two design filters that determine a set of scalable optimal designs to be considered for further development. The first filter retains designs that dominate in terms of performance throughout the parameter space (set of parametric optimal designs $\mathbf{X}^*$). The second filter retains designs that are scalable by remanufacturing (scalable design set $\mathbf{X}_s$). The number of samples for the KS response surface is chosen such that the order-based error is minimized with respect to a validation set. The methods developed in this section are now applied to an industrial case study.

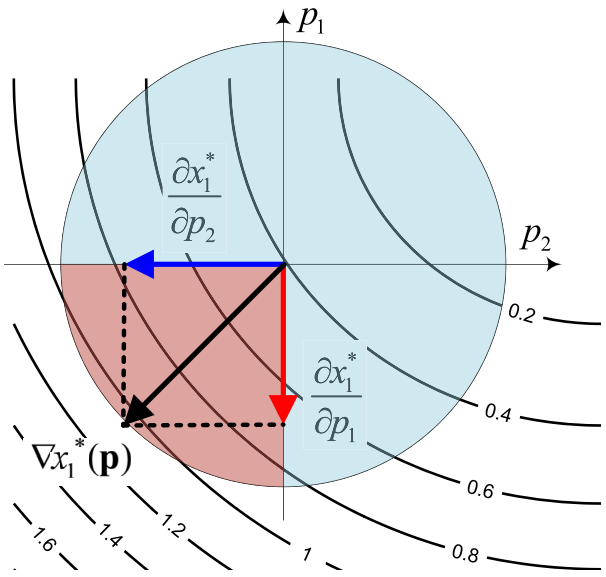


**Fig. 2 Isocontours of the response surface $x_1{}^*(\mathbf{p})$ and transition rule $\mathbf{N}\,\mathbf{J}^T(\mathbf{p})\mathbf{M} \geq \mathbf{0}$ in a two-dimensional parameter space**

## 4 Application Example: Aeroengine Component Remanufacturing

A turbine rear structure (TRS) is a structural aeroengine component at the turbine exhaust. It must sustain thermal and structural loads during flight due to exhaust gases while mounting the engine to the wing structure. Analysis of the component in the industry involves multiple disciplines (aerodynamic, structural, and thermal).

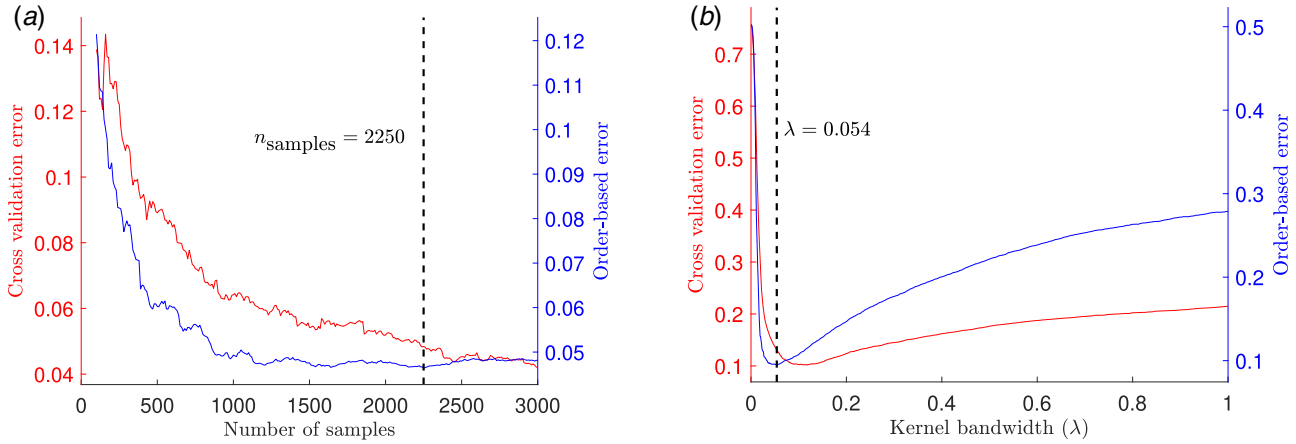


**Fig. 3 Effect of number of training points and kernel bandwidth on order-based error: (*a*) sampling effect and (*b*) bandwidth effect**

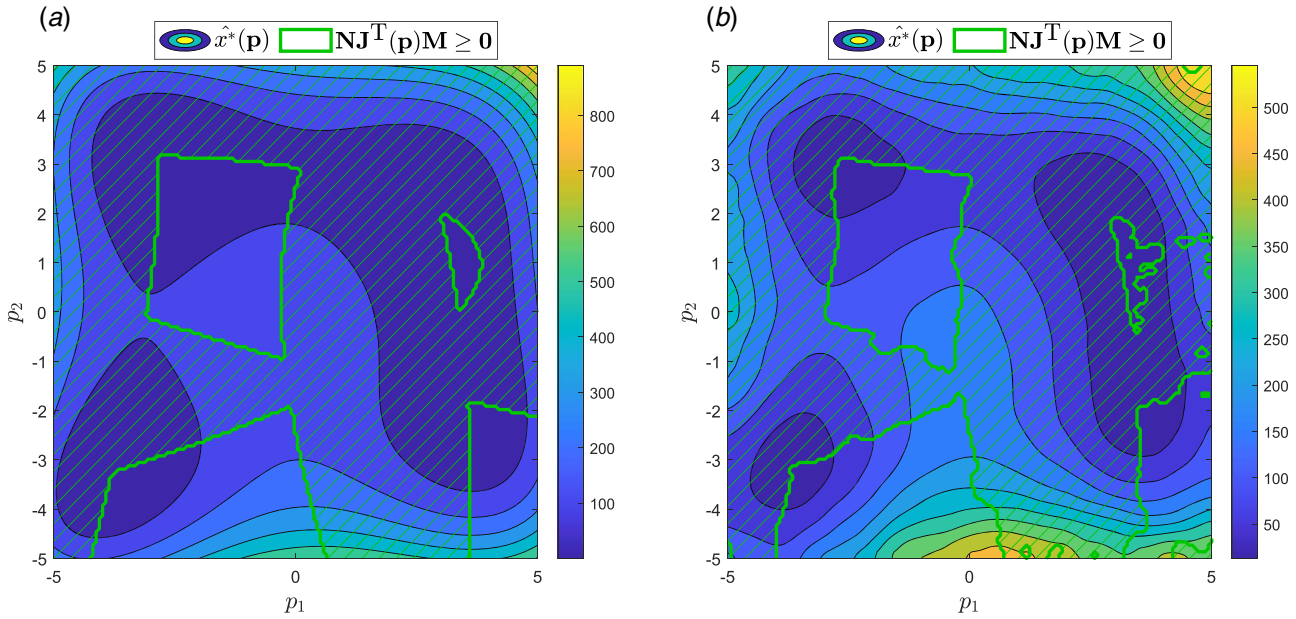


**Fig. 4 Approximation of scalable set using KS with non-scalable regions of the parameter space hatched: (*a*) test function and (*b*) KS approximation**

We consider the deposition of a stiffener on the TRS to support higher loading requirements. The first step of the analysis involves a thermomechanical model to compute the residual stresses in the structure ($\sigma_{v1}$). Next, a pressure load is applied on the outer casing resulting in a new stress state ($\sigma_{v2}$). The mean and amplitude of the initial and final stress states are used to compute the safety factor against low-cycle fatigue as a structural performance requirement.

The following section outlines the thermomechanical models used to predict the residual stresses that result from the AM deposition process.

**4.1 Thermomechanical Modeling.** The directed energy deposition (DED) of the stiffener increases the thickness of the outer casing as shown in Fig. 5.

Comprehensive thermomechanical models feature a coupled transient heat transfer and fluid flow model to accurately calculate the transient temperature field. The temperature field is used for residual stress and distortion modeling [59]. Complex physical processes govern the temperature field making its computation intensive. Computations of the temperature field involve various simplifications and assumptions to make the calculations tractable. Manvatkar et al. [60] consider a finite element analysis (FEA) conduction model for calculating the transient temperature field due to a moving Gaussian heat source on the substrate. The problem of a moving heat source on an infinite plate was formulated and solved analytically by Rosenthal [61]. The Rosenthal model is used for cases where there is limited heat conduction in the through thickness dimension typical of thin plates [62]. The TRS outer casing where the stiffener is to be deposited has a through thickness dimension considerably smaller than its width and circumference allowing us to approximate the heat source by a Gaussian heat source as in the Rosenthal model.

The melt pool dimensions are estimated from the transient thermal model to determine the deposit width and depth. Figure 6 shows the details of the thermomechanical simulations for determining deposit size. A Gaussian heat source with a heat flux distribution given by Eq. (15) scans the surface at a constant speed $V$ [61]

$$Q(r,\theta,t) = \frac{P}{\pi r_l^2 D} e^{-2\left(\frac{r-Vt}{r_l}\right)^2} \tag{15}$$

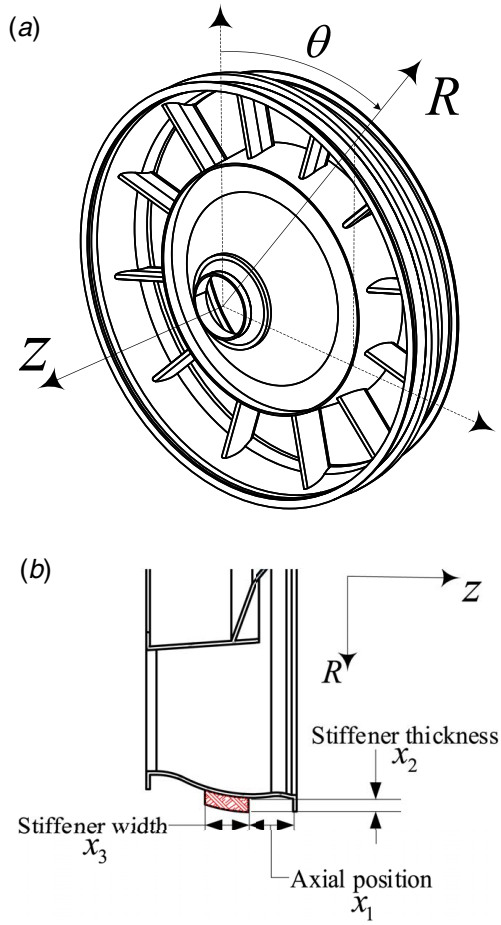


**Fig. 5 TRS stiffener example: (*a*) TRS schematic and (*b*) deposition variables**

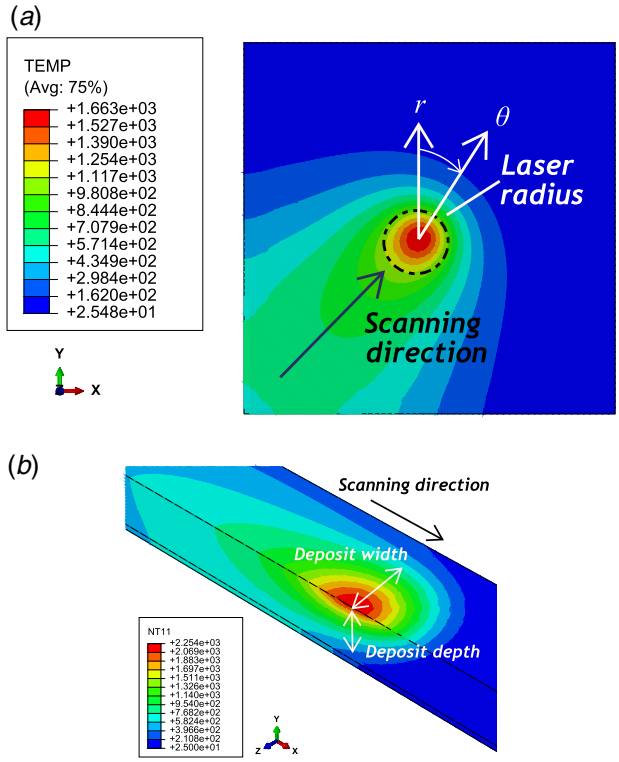


**Fig. 6 Heat conduction for a moving Gaussian heat source: (*a*) Gaussian heat source and (*b*) melt pool**

where $r_l$ is the laser beam radius, $P$ is the laser power, and $D$ is the depth of penetration of the laser source. The coordinates $r$ and $\theta$ are defined on the surface of the deposit as shown in Fig. 6(*a*).

The resulting deposit width $D_w$ and depth $D_d$ are used to partition the stiffener geometry into $n_l$ by $n_d$ deposits in the axial and radial directions, respectively, where $n_l = \lfloor x_3/D_w \rceil$ and $n_d = \lfloor x_2/D_d \rceil$.

For the deposition on the TRS outercasing, a further simplification of the transient conduction model can be made by applying the heat flux uniformly on the surface of the deposit [63]. We use a static model with a uniformly distributed heat flux to compute residual stresses. This idealization (relative to using a transient heat transfer model) reduces the number of variables and parameters involved and alleviates computational cost by exploiting TRS symmetry without sacrificing accuracy excessively.

Each deposit is heated uniformly by an equivalent heat flux that supplies the same energy as a moving Gaussian heat source scanning the entire deposit surface. The power at $t=0$ is given by the surface integral of the heat flux over an infinite plane

$$P(t=0) = \frac{P}{\pi r_l^2 D}\int_0^{2\pi}\int_0^{\infty} e^{-2\left(\frac{r}{r_l}\right)^2} r\,dr\,d\theta = \frac{P}{\pi r_l^2 D}\frac{\pi r_l^2}{2} = \frac{P}{2D} \tag{16}$$

The power per unit depth $P(t=0)$ is multiplied by the time $t=L/V$, where $L=2\pi R_{\text{outer}}$ and $R_{\text{outer}}=0.5$ m is the radius of the outer casing of the TRS to obtain the heat energy input to the deposit. The energy is divided by an equivalent step time $t_{\text{step}}$ used for static thermal analysis in lieu of a transient thermal analysis to obtain the equivalent uniformly distributed power per unit depth $P_{\text{eqv}}$. Finally, $P_{\text{eqv}}$ is divided by the area of the deposit ($A_{\text{deposit}} = 2\pi R_{\text{outer}} D_w$) to yield the equivalent heat flux per unit depth $Q_{\text{eqv}}$

$$\begin{aligned} Q_{\text{eqv}} &= P(t=0)\frac{2\pi R_{\text{outer}}}{V}\frac{1}{t_{\text{step}}}\frac{1}{2\pi R_{\text{outer}} D_w} \\ &= P(t=0)\frac{1}{V t_{\text{step}} D_w} = \frac{P}{2V t_{\text{step}} D_w D} \end{aligned} \tag{17}$$

We assume here that the radius of the deposit is equal to the radius of the outer casing $R_{\text{outer}}$ since the thickness of the deposit is small relative to the outer casing.

The application of $Q_{\text{eqv}}$ to the surface of a deposit layer is shown in Fig. 8(*a*). After obtaining the thermal gradients due to the application of the heat flux load, the corresponding thermal stresses are computed. The stresses that persist after removal of the heat flux load are the residual stresses. These residual stresses are inherent in the structure and affect the structural performance of the TRS during subsequent operational loads. The maximum and minimum residual principal stresses along the circumference of the TRS outer casing are shown in Fig. 7 for both static and transient models. The principal stresses provide an indication of the compressive or tensile nature of the stress state and will be used in subsequent failure analysis to determine the safety factor. There is a general agreement in the value of the predicted stresses with lower values recorded for the transient model due to the time taken by the substrate to reach steady-state temperatures as the heat source scans its surface. Furthermore, the static model overpredicts the maximum principal stress making it a more conservative choice for thermomechanical modeling.

A pressurization/depressurization load case due to the exhaust gas pressure ($P_{\text{load}}$) cycle is shown in Fig. 8(*b*). The load case is cycled and is used to compute the expected fatigue life of the TRS using low-cycle fatigue calculations. The stress state at the foot of a strut (shown in Fig. 8(*b*)) is monitored before and after the load case to obtain the initial and final Von mises stresses $\sigma_{v1}$ and $\sigma_{v2}$, respectively. Note that $\sigma_{v1} \neq 0$ due to the residual stress

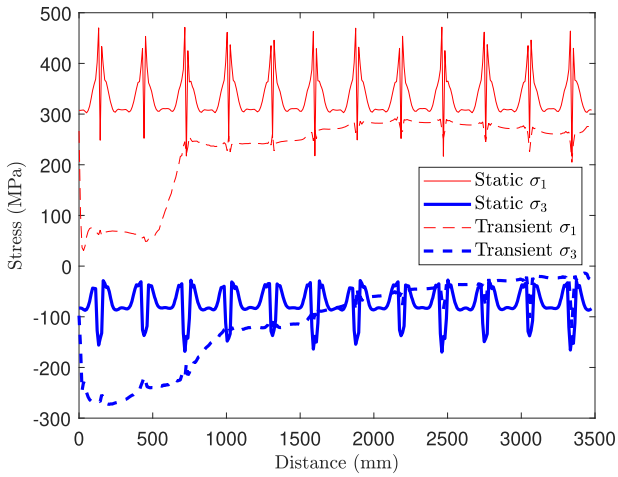


**Fig. 7 Spatial distribution of principle residual stresses along the circumference of the TRS obtained using transient and static models**

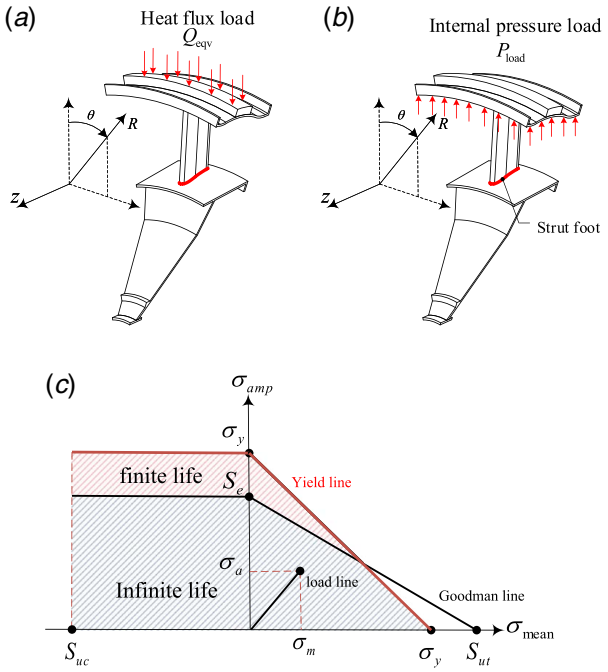


**Fig. 8 TRS thermomechanical loads: (*a*) deposition load, (*b*) pressure load case, and (*c*) modified Goodman criterion**

state in the structure from prior thermomechanical loads. The mid-range stress ($\sigma_m = -\text{sign}(\sigma_P)(\sigma_{v1} + \sigma_{v2})/2$) and the amplitude stress ($\sigma_a = |\sigma_{v1} - \sigma_{v2}|/2$) are calculated, where $\text{sign}(\sigma_P)$ is the sign of the pressure given by the sum of the principle stresses ($\sigma_P = -(1/3)(\sigma_1 + \sigma_2 + \sigma_3)$) and provides of measure of the compressive or tensile state of the stress. A negative $\sigma_P$ implies tension while a positive value implies compression. The failure locus is determined by the modified Goodman criterion for high cycle fatigue as shown in Fig. 8(*c*). The endurance limit ($S_e$), yield stress ($\sigma_y$), and ultimate strength ($S_{ut}$) are defined as parameters and are obtained from mechanical design handbooks [64]. The number of lifecycles to failure is estimated from Wöhler relations ($N_f = (\sigma_{\text{rev}}/a)^b$), where $a$ and $b$ are empirical constants. The safety factor is calculated as $n_{\text{safety}} = 1 \Big/ \left(\frac{\sigma_a}{S_e} + \frac{\sigma_m}{S_{ut}}\right)$ for each load case.

**Table 1 Comparison of transient and static models: parameter values**

| Parameter | Notation | Units | Value |
|---|---|---|---|
| Stiffener axial position | $x_1$ | mm | 80.0 |
| Stiffener thickness | $x_2$ | mm | 4.0 |
| Stiffener width | $x_3$ | mm | 23.5 |
| Laser power | $P$ | W | 3,889.13 |
| Laser beam radius | $r_l$ | mm | 13.63 |
| Scanning speed | $V$ | mm/s | 5.0 |
| Number of layers | $n_l$ | – | 2 |
| Number of deposits (transverse) | $n_d$ | – | 1 |
| Deposit depth | $D_d$ | mm | 2.01 |
| Deposit width | $D_w$ | mm | 25.0 |
| Deposit surface area | $A_{\text{deposit}}$ | $\text{mm}^2$ | $8.304 \times 10^4$ |
| Equivalent heat flux per unit depth | $Q_{\text{eqv}}$ | $\text{W/mm}^3$ | 0.8138 |

The scanning speed is considered constant at a nominal value of $V = 5$ mm/s. Exploiting symmetry, only one sector of the TRS is analyzed, which reduces the computational domain and effort significantly. We compare the results obtained by transient and static models for a sample case to obtain an understanding of the prediction discrepancies. Table 1 summarizes the utilized parameter values.

The remanufacturing model is summarized in Tables 2–4 to facilitate the formulation of the optimization problem for SBD in Sec. 4.2.

**4.2 Problem Formulation.** The design optimization problem is formulated as

$$\begin{aligned} \min_{\mathbf{x}^{\mathrm{T}}=[x_1,x_2,x_3,P]} \quad & f(\mathbf{x};\mathbf{p}) = -n_{\text{safety}}(P_{\text{load}}) \\ \text{subject to} \quad & g_1(\mathbf{x};\mathbf{p}) = x_3 + x_1 - W_{\text{total}} \le 0 \\ & g_2(\mathbf{x};\mathbf{p}) = T_m - T_{\text{deposit}} \le 0 \end{aligned} \tag{18}$$

where $n_{\text{safety}}$ is the safety factor against low cycle fatigue or first cycle yielding for the load case. The constraints pertain to the substrate width on the outer casing (the region where deposition is permitted) and the melting temperature of the deposit material needed to consolidate the material.

**4.3 Parametric Optimal Design Results.** The design optimization problem in Eq. (18) is solved using the mesh adaptive direct search (MADS) algorithm. We use the `OrthoMADS` implementation provided by the `NOMAD` algorithm [65]. The termination criterion for MADS was the minimum mesh size (defined by Audet and Dennis [66]) reached in the virtually discretized design variable space. Non-opportunistic Latin hypercube search was used during the search step. A progressive barrier approach was used for handling constraints. This choice of algorithm is motivated by the possible non-existence of gradients or the inability to approximate them with reasonable computational cost and warranted due to its rigorous convergence properties.

As described earlier, Latin hypercubes are used to sample the design and parameters spaces defined by the bounds and ranges of the design variables and parameters, respectively (see Tables 2 and 3).

For our numerical investigations, the design optimization problem is solved for 1200 LH samples of the parameter space to obtain a set of parametric optimal design solutions. Up to 900 samples are used as a training set for the KS model, while the remaining 300 are reserved for use as a validation set to check the order-based error. The effect of the parameters on the optimizer is illustrated by three sample results shown in Fig. 9 (see Table 5).

These three samples have been chosen to include one interior optimal design (Fig. 9(*a*)), one boundary optimal design with one active constraint (Fig. 9(*b*)), and one boundary optimal design with two active constraints (Fig. 9(*c*)). The optimizers obtained

**Table 2 Design variables x**

| Design variable | Notation | Units | Lower bound | Upper bound | Mono-tonicity |
|---|---|---|---|---|---|
| Stiffener axial position | $x_1$ | mm | 37 | 145 | 0 |
| Stiffener thickness | $x_2$ | mm | 2 | 10 | 1 |
| Stiffener width | $x_3$ | mm | 10 | 40 | 1 |
| Laser power | $P$ | W | 3,500 | 4,000 | 0 |

**Table 3 Design parameters p**

| Parameter | Notation | Units | Range | Change agent |
|---|---|---|---|---|
| Internal pressure load | $P_{\text{load}}$ | MPa | $2 \pm 0.5$ | 1 |
| Deposit melting point | $T_m$ | °C | $1,500 \pm 100$ | −1 |
| Substrate base width | $W_{\text{total}}$ | mm | $137.5 \pm 17.5$ | −1 |

**Table 4 Relevant model outputs**

| Output | Notation | Units |
|---|---|---|
| Number of layers | $n_l$ | – |
| Number of deposits (transverse) | $n_d$ | – |
| Deposit depth | $D_d$ | mm |
| Deposit length | $D_l$ | mm |
| Deposit width | $D_w$ | mm |
| Deposit surface area | $A_{\text{deposit}}$ | $\text{mm}^2$ |
| Equivalent heat flux | $Q_{\text{eqv}}$ | $\text{W/mm}^2$ |
| Safety factor at strut foot (IP load) | $n_{\text{safety}}$ | – |
| Number of lifecycles to failure ($P_{\text{load}}$) | $N_f$ | – |
| Deposition temperature | $T_{\text{deposit}}$ | °C |

by sampling the parameter space are used to construct a convex hull to quantify the size of the set of parametric optimal designs. The `qhull` algorithm was used to construct the four-dimensional polygon (polytope) characterizing the convex hull [67].

**4.4 Scalable Optimal Design Results.** Of the 900 parametric optimal designs obtained by solving the optimization problem for different parameter values, 592 samples were used to construct a response surface that can predict a parametric optimal design for other parameter values. As explained in Sec. 3.4, the order-based error relative to a validation set was minimized to determine the number of training samples. The kernel bandwidth ($\lambda$) was determined to be 0.71. This result is shown in Fig. 11.

Designs meeting scalability requirements in the parameter space are identified using the scalability constraint in Sec. 3.3. The monotonicity vector is defined as $\mathbf{m} = [0\ 1\ 1\ 0]^{\text{T}}$ for the variables in Table 2. The change agent vector is defined as $\mathbf{n} = [1\ -1\ -1]^{\text{T}}$. As an illustrative example, the two-dimensional projections of the parameter space for the optimal width design variable are depicted in Fig. 10.

The scalability transition rule results in pockets within the parameter space that can be mapped back to design space by evaluating the optimizer response surface within these pockets. The parameter space is sampled using a full factorial grid and designs meeting the scalability constraint are tabulated and projected on the design space in Fig. 12(*a*).

The convex hull formed by the scalable optimal designs is considerably smaller in volume than that formed by the set of parametric optimal designs.

The set of scalable optimal designs can be enlarged to include more designs be relaxing some of the scalability constraints. We relax all the constraints with respect to the thickness design variable $x_2$ by setting the monotonicity with respect to $x_2$ to 0. The monotonicity vector becomes $\mathbf{m} = [0\ 0\ 1\ 0]^{\text{T}}$. The result of this relaxation is shown in Fig. 12(*b*).

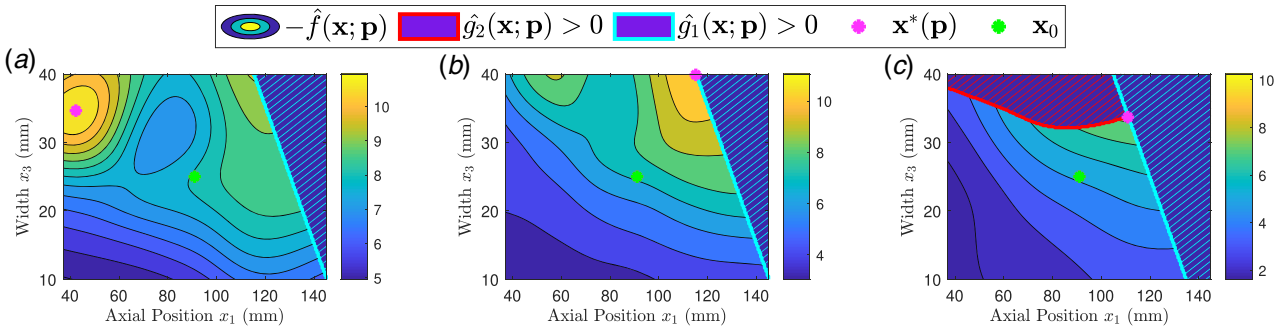


**Fig. 9 Three sample parametric optimal designs; $\mathbf{x}_0$ denotes the baseline design: (*a*) $\mathbf{p}_1$, (*b*) $\mathbf{p}_2$, and (c) $\mathbf{p}_3$**

**Table 5 Sample optimization problem results**

| | | Parameters | | | | | | | | |
|---|---|---|---|---|---|---|---|---|---|---|
| | | $\mathbf{p}_1$ | | | $\mathbf{p}_2$ | | | $\mathbf{p}_3$ | | |
| Result | Units | $P_{\text{load}}$ (MPa) | $T_m$ (°C) | $W_{\text{total}}$ mm | $P_{\text{load}}$ (MPa) | $T_m$ (°C) | $W_{\text{total}}$ mm | $P_{\text{load}}$ (MPa) | $T_m$ (°C) | $W_{\text{total}}$ mm |
| | | 1.87 | 1,400 | 155 | 2.08 | 1,400 | 155 | 2.3973 | 1,427 | 145 |
| $x_1^*$ | mm | | 42.2 | | | 115.1 | | | 110.9 | |
| $x_2^*$ | mm | | 10.0 | | | 9.0 | | | 8.8 | |
| $x_3^*$ | mm | | 34.7 | | | 39.9 | | | 33.7 | |
| $P^*$ | W | | 3,500 | | | 3,770 | | | 3,991 | |
| $g_1(\mathbf{x}^*)$ | mm | | −78.1 | | | 0 (active) | | | 0 (active) | |
| $g_2(\mathbf{x}^*)$ | °C | | −393 | | | −381 | | | 0 (active) | |
| $f(\mathbf{x}^*)$ | – | | −11 | | | −11 | | | −8 | |

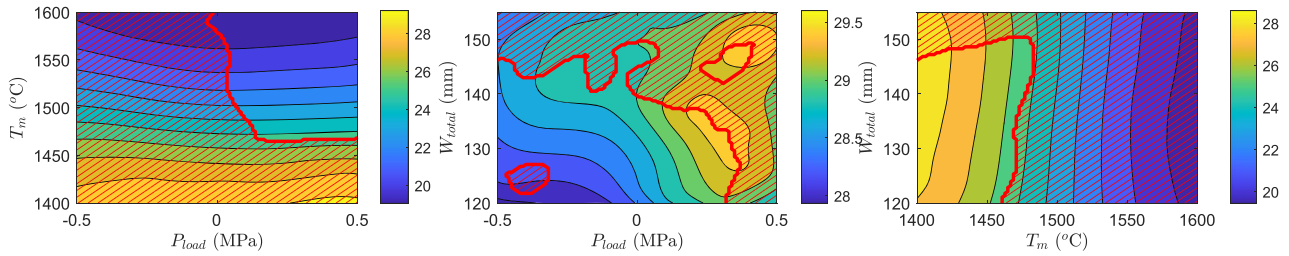


**Fig. 10 Projections of the optimal width design variable $\hat{x}_3^*$ with non-scalable regions of the parameter space hatched**

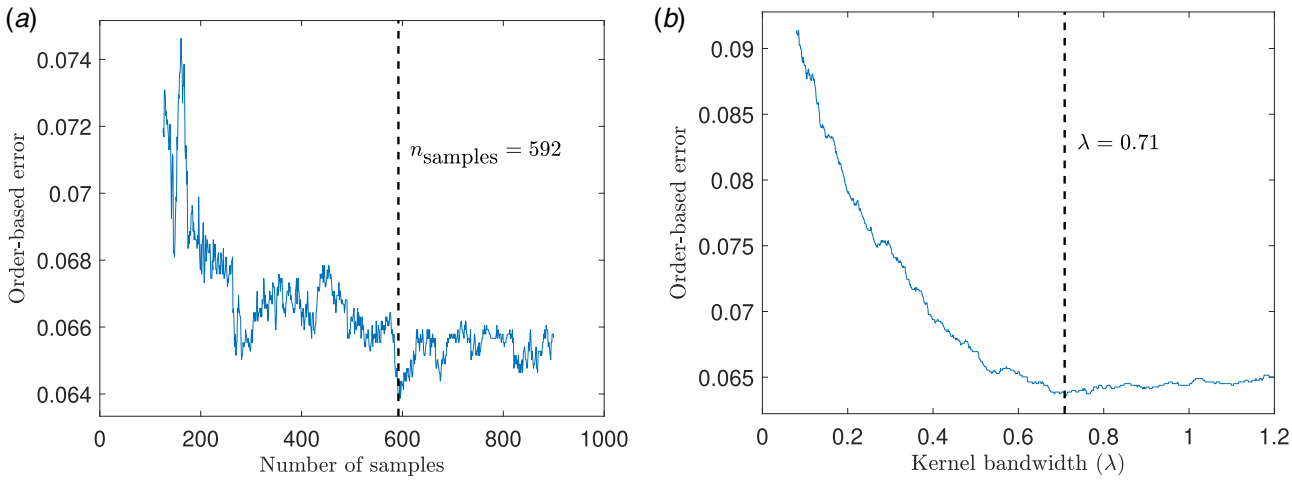


**Fig. 11 Effect of number of training points and kernel bandwidth on order-based error: (*a*) sampling effect and (*b*) bandwidth effect**

Adhering to scalability constraints allows designers the flexibility to scale designs as parameters evolve even after commitment by considering remanufacturing scenarios. Figure 10 shows this scenario as the contours of $\hat{x}_3^*$ increase in value for any vector contained within the change agent hyperoctant as defined by **n**.

**4.5 Design Set Variability and Comparison.** Having generated the feasible design set, the set of parametric optimal design, and the set of scalable optimal designs for the TRS remanufacturing problem, some comparisons can be made. Several metrics exist in the literature for comparing the variability of a design solution set generated by parametric optimal design tools such as those formulated in this paper. The volume of the convex hull provides a good perception of design variability provided that there are sufficient points to construct the polytope characterizing the convex hull [68]. The convex hull volume was used to compare the reduction in the design sets as our methodology was applied to the TRS problem. The lower and upper bounds (LB and UB, respectively) of the ranged set containing each solution set are also found. They are used to compute the volume of the bounding hyper-rectangle. The hyper-rectangle volume provides a benchmark against the ranged set representation used for previous SBD studies [25,28,29,32,37].

Table 6 summarizes the results of this comparison. It can be seen that a significant reduction of the design space was caused by each set-based filter step of our methodology. This is because smaller values for the laser power $P$ and thickness $x_2$ resulted in consistently suboptimal designs with respect to performance. However, among the scalable designs many featured axial positions ($x_1$) and widths ($x_3$) near the upper and lower bounds for each variable, respectively. This is due the positive monotonicity of the volume with respect to $x_3$. Such designs have the greatest potential for scalability. The relative volume of the convex hull to that of the design space is calculated in the last row of the table. The design space volume was normalized to 1 for ease of comparison. Feasible solutions comprised about three-fourths of the design space (77.%). The parametric optimal design solutions comprised only 2.8%. The scalable solutions obtained for $\mathbf{m} = [0\ 1\ 1\ 0]^T$ and $\mathbf{m} = [0\ 0\ 1\ 0]^T$ comprised $6.3 \times 10^{-7}$% and 0.00104% of the design space, respectively. While these proportions may seem small, they are significant in size in the considered four-dimensional design space. For comparison, the volume of the hyper-rectangle enclosing the design sets was also calculated since most of the surveyed set-based design methods used hyper-rectangles to prescribe their solution sets. The design variable bounds where normalized relative to the upper and lower bounds of the design space and corresponding volume was computed by finding the product of the length of the "edges" of the hyper-rectangle. It can be seen that the hyper-rectangle overestimates the volume of the design sets due to its inability to capture the arbitrary shape of the different design sets shown in Fig. 12.

The results of this remanufacturing case study demonstrate the usefulness of the transition rule formulated in this paper for providing scalable remanufacturing design solutions for a range of design requirements. By accommodating variability in the design stage and incorporating flexible design principles, future potential losses in raw material and manufacturing effort are alleviated by avoiding disposal and replacement scenarios. Even previously commissioned components can be scaled by our methodology as shown in this paper by carefully designing the remanufactured additions to the component. This will ensure continued scalability of the component in the future.

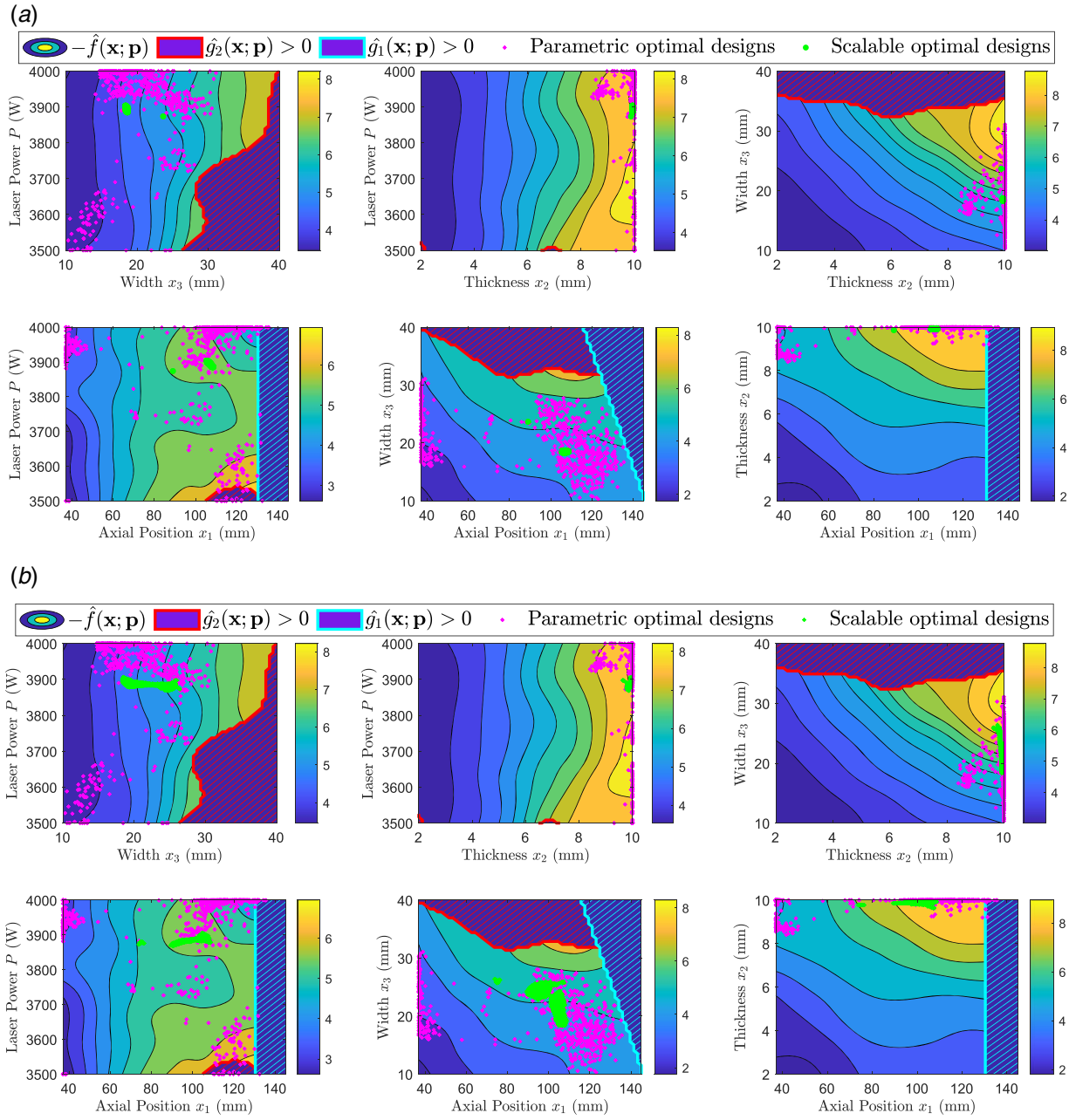


**Fig. 12 Safety factor in the feasible design space as a function of design variables for different monotonicity vectors: (*a*) $\mathbf{m} = [0\ 1\ 1\ 0]^T$, $\mathbf{n} = [1\ -1\ -1]^T$ and (*b*) $\mathbf{m} = [0\ 0\ 1\ 0]^T$, $\mathbf{n} = [1\ -1\ -1]^T$**

**Table 6 Design space comparison results**

| | Feasible design space | | Set of parametric optimal designs | | Scalable design set | | | |
|---|---|---|---|---|---|---|---|---|
| | | | | | $\mathbf{m} = [0\ 1\ 1\ 0]^T$ $\mathbf{n} = [1\ -1\ -1]^T$ | | $\mathbf{m} = [0\ 0\ 1\ 0]^T$ $\mathbf{n} = [1\ -1\ -1]^T$ | |
| Quantity | LB | UB | LB | UB | LB | UB | LB | UB |
| $x_1$ | 37 | 145 | 37 | 136 | 88.9 | 108.6 | 73.7 | 108.7 |
| $x_2$ | 2 | 10 | 8.4 | 10 | 9.8 | 9.9 | 9.6 | 9.9 |
| $x_3$ | 10 | 40 | 10.3 | 31.1 | 18.3 | 23.7 | 18.3 | 26.4 |
| $P$ | 3500 | 4000 | 3500 | 4000 | 3874 | 3904 | 3869 | 3907 |
| $V_{\text{hyper-rectangle}}$ | 1 | | 0.13 | | 0.0016 | | 0.0025 | |
| $V_{\text{convhull}}$ | 0.77 | | 0.028 | | $6.3 \times 10^{-9}$ | | $1.04 \times 10^{-5}$ | |
| Relative volume | 77% | | 2.8% | | $6.3 \times 10^{-7}$% | | 0.00104% | |

## 5 Conclusion and Future Work

We presented a set-based design methodology that utilizes surrogate-assisted numerical optimization, post-optimality analysis, and monotonicity-driven transition rules related to additive or subtractive manufacturing to generate a set of scalable optimal designs. This methodology can be used either for considering several different alternative solutions during initial design stages where requirements are still open-ended or, in combination with remanufacturing, to implement redesigns that can satisfy changed requirements, extending thus the useful lifetime of components and systems.

The methodology was applied to an aero-engine component design case study: a set of parametric optimal design solutions was generated and scalable design solutions were successfully extracted. Since we are only considering a finite, albeit large, amount of designs, we used convex hulls to quantify approximately the cardinality of the sets in order to make relative comparisons among them.

The scalability assessment assumed monotonicity of component volume in the considered design variables, which is not uncommon in many engineering design and remanufacturing problems. Nevertheless, the scalability assessment presented here may be extendable to include nonmonotonic variables by performing localized monotonicity assessments in the design space.

This work enables design changes by remanufacturing through the derived transition rules. The formulated optimization problem is driven by thermomechanical performance requirements that impact its useful lifetime and how it can be extended. However, changeability aspects should include cost, especially as this relates directly to the lifecycle of the component and its importance to circular economy principles. A changeability cost threshold must be observed by designers when making remanufacturing decisions and should be integrated into any future transition rules [26]. Future studies could also focus on other product recovery activities along the innermost circles of a CE such as repair and reuse as they may preserve valuable resources more efficiently than remanufacturing. Nevertheless, these options need not be mutually exclusive.

Finally, requirements specific to the condition of the component core to be remanufactured were not considered here; e.g., the severity of component wear and tear at the time of remanufacturing. This is a highly variable condition that needs to be taken into account in our methodology as it can impact the generated solution sets significantly. In addition to the condition of the core, the operational history of the core could add another dimension to the design problem in terms of variability. Uncertainty quantification methods may offer paradigms to address this issue.


## Acknowledgment

The first and last authors are grateful for the partial support of their work by grants NSERC CRDPJ 479630-15 X-243027 and CARIC CRDPJ479630-15 X-243067. The first author is grateful for the partial support of FRQNT through the *Bourses de doctorat en recherche* program (file 273486). The first author is grateful to the Faculty of Engineering at McGill University for its partial support through a McGill Engineering Doctoral Award. The work of the second author has been partially supported by a European Union Horizon 2020 research and innovation programme under grant agreement 690608. Support from the Area of Advanced Production at Chalmers is also acknowledged. None of the aforementioned partial financial support does constitute in any way an endorsement of the opinions expressed in this paper. Finally, the first and last authors would like to express their gratitude to the Department of Industrial and Materials Science at Chalmers University of Technology for its hospitality during extended research visits.


## Conflict of Interest

There are no conflicts of interest.

## Data Availability Statement

The datasets generated and supporting the findings of this article are obtainable from the corresponding author upon reasonable request. The authors attest that all data for this study are included in the paper. Data provided by a third party are listed in Acknowledgment.

## References


[1] Matos, S., and Hall, J., 2007, "Integrating Sustainable Development in the Supply Chain: The Case of Life Cycle Assessment in Oil and Gas and Agricultural Biotechnology," J. Oper. Manage., **25**(6), pp. 1083–1102.

[2] Neto, J., Walther, G., Bloemhof, J., Van Nunen, J., and Spengler, T., 2010, "From Closed-loop to Sustainable Supply Chains: The WEEE Case," Int. J. Prod. Res., **48**(15), pp. 4463–4481.

[3] Lieder, M., and Rashid, A., 2016, "Towards Circular Economy Implementation: A Comprehensive Review in Context of Manufacturing Industry," J. Cleaner. Prod., **115**, pp. 36–51.

[4] Ellen Macarthur Foundation, 2012, Towards the Circular Economy: An Economic and Business Rationale for an Accelerated Transition, Technical Report.

[5] Ijomah, W., McMahon, C., Hammond, G., and Newman, S., 2007, "Development of Robust Design-for-Remanufacturing Guidelines to Further the Aims of Sustainable Development," Int. J. Prod. Res., **45**(18–19), pp. 4513–4536.

[6] Liu, J., and Ma, Y., 2016, "Sustainable Design-Oriented Level Set Topology Optimization," ASME J. Mech. Des., **139**(1), p. 011403.

[7] Mahadevan, B., Pyke, D., and Fleischmann, M., 2003, "Periodic Review, Push Inventory Policies for Remanufacturing," Eur. J. Oper. Res., **151**(3), pp. 536–551.

[8] Golinska, P., Kosacka, M., Mierzwiak, R., and Werner-Lewandowska, K., 2015, "Grey Decision Making As a Tool for the Classification of the Sustainability Level of Remanufacturing Companies," J. Cleaner. Prod., **105**, pp. 28–40.

[9] Van-Thao, L., Paris, H., and Mandil, G., 2015, "Using Additive and Subtractive Manufacturing Technologies in a New Remanufacturing Strategy to Produce New Parts From End-of-Life Parts," 22ème Congrès Français de Mécanique CFM2015, Lyon, France, Aug. 24–28.

[10] Song, C., Guan, X., Zhao, Q., and Ho, Y., 2005, "Machine Learning Approach for Determining Feasible Plans of a Remanufacturing System," IEEE Trans. Auto. Sci. Eng., **2**(3), pp. 262–275.

[11] Koren, Y., Gu, X., Badurdeen, F., and Jawahir, I., 2018, "Sustainable Living Factories for Next Generation Manufacturing," 15th Global Conference on Sustainable Manufacturing, Haifa, Israel, Sept. 25–27.

[12] Goodall, P., Rosamond, E., and Harding, J., 2014, "A Review of the State of the Art in Tools and Techniques Used to Evaluate Remanufacturing Feasibility," J. Cleaner. Prod., **81**, pp. 1–15.

[13] Lindahl, M., Sundin, E., Östlin, J., and Björkman, M., 2007, "Concepts and Definitions for Product Recovery Analysis and Clarification of the Terminology used in Academia and Industry," *Innovation in Life Cycle Engineering and Sustainable Development*, D. Brissaud, S. Tichkiewitch, and P. Zwolinski, eds., Springer Netherlands, Dordrecht, pp. 123–138.

[14] Thierry, M., Salomon, M., Van Nunen, J., and Van Wassenhove, L., 1995, "Strategic Issues in Product Recovery Management," California Manage. Rev., **37**(2), pp. 114–136.

[15] Remanufacturing Industries Council, 2017. Specifications for Process of Remanufacturing. Technical Report.

[16] Fricke, E., and Schulz, A., 2005, "Design for Changeability (DfC): Principles to Enable Changes in Systems Throughout Their Entire Lifecycle," Syst. Eng., **8**(4), pp. 342–359.

[17] De Neufville, R., and Scholtes, S., 2011, *Flexibility in Engineering Design*, MIT Press, London.

[18] Leino, M., Pekkarinen, J., and Soukka, R., 2016, "The Role of Laser Additive Manufacturing Methods of Metals in Repair, Refurbishment and Remanufacturing—Enabling Circular Economy," 9th International Conference on Photonic Technologies, Fürth, Germany, Sept. 19–22.

[19] Kellens, K., Baumers, M., Gutowski, T., Flanagan, W., Lifset, R., and Duflou, J., 2017, "Environmental Dimensions of Additive Manufacturing: Mapping Application Domains and Their Environmental Implications," J. Ind. Ecology, **21**(S1), pp. S49–S68.

[20] Ijomah, W. L., 2009, "Addressing Decision Making for Remanufacturing Operations and Design-for-Remanufacture," Int. J. Sustainable Eng., **2**(2), pp. 91–102.

[21] Wilson, J. M., Piya, C., Shin, Y. C., Zhao, F., and Ramani, K., 2014, "Remanufacturing of Turbine Blades by Laser Direct Deposition With Its Energy and Environmental Impact Analysis," J. Cleaner. Prod., **80**, pp. 170–178.

[22] Tang, Y., Mak, K., and Zhao, Y., 2016, "A Framework to Reduce Product Environmental Impact Through Design Optimization for Additive Manufacturing," J. Cleaner. Prod., **137**, pp. 1560–1572.

[23] Xing, K., Belusko, M., Luong, L., and Abhary, K., 2007, "An Evaluation Model of Product Upgradeability for Remanufacture," Int. J. Adv. Manuf. Technol., **35**(1–2), pp. 1–14.

[24] Kwak, M., and Kim, H., 2013, "Market Positioning of Remanufactured Products with Optimal Planning for Part Upgrades," ASME J. Mech. Des., **135**(1), p. 011007.

[25] Suh, E. S., De Weck, O. L., and Chang, D., 2007, "Flexible Product Platforms: Framework and Case Study," Res. Eng. Design, **18**(2), pp. 67–89.
[26] Ross, A., Rhodes, D., and Hastings, D., 2008, "Defining Changeability: Reconciling Flexibility, Adaptability, Scalability, Modifiability, and Robustness for Maintaining System Lifecycle Value," Syst. Eng., **11**(3), pp. 246–262.
[27] Tackett, M. W., Mattson, C. A., and Ferguson, S. M., 2014, "A Model for Quantifying System Evolvability Based on Excess and Capacity," ASME J. Mech. Des., **136**(5), p. 051002.
[28] Olewnik, A., Brauen, T., Ferguson, S., and Lewis, K., 2004, "A Framework for Flexible Systems and Its Implementation in Multiattribute Decision Making," ASME J. Mech. Des., **126**(3), pp. 412–419.
[29] Liu, H., Chen, W., Scott, M. J., and Qureshi, K., 2008, "Determination of Ranged Sets of Design Specifications by Incorporating Design-space Heterogeneity," Eng. Optim., **40**(11), pp. 1011–1029.
[30] Ferguson, S., Lewis, K., Siddiqi, A., and De Weck, O. L., 2008, "Flexible and Reconfigurable Systems: Nomenclature and Review," 2007 Proceedings of the ASME International Design Engineering Technical Conferences and Computers and Information in Engineering Conference DETC2007, Las Vegas, NV, Sept. 4–7, Vol. 6 PART A, pp. 249–263.
[31] Yannou, B., Simpson, T. W., and Barton, R. R., 2003, "Towards a Conceptual Design Explorer Using Metamodeling Approaches and Constraint Programming," Proceedings of the ASME Design Engineering Technical Conference, Vol. 2 Part A of International Design Engineering Technical Conferences and Computers and Information in Engineering Conference, Chicago, IL, Sept. 2–6, pp. 605–614.
[32] Qureshi, A., Dantan, J.-Y., Bruyere, J., and Bigot, R., 2014, "Set-Based Design of Mechanical Systems with Design Robustness Integrated," Int. J. Product Dev., **19**(1/2/3), p. 64.
[33] Kerga, E., Rossi, M., Taisch, M., and Terzi, S., 2014, "A Serious Game for Introducing Set-Based Concurrent Engineering in Industrial Practices," Concurrent Eng. Res. Appl., **22**(4), pp. 333–346.
[34] Sobek II, D., Ward, A., and Liker, J., 1999, "Toyota's Principles of Set-Based Concurrent Engineering," MIT Sloan Manage. Rev., **40**(2), pp. 67–83.
[35] Levandowski, C., Michaelis, M., and Johannesson, H., 2014, "Set-Based Development Using An Integrated Product and Manufacturing System Platform," Cconcurrent Eng. Res. Appl., **22**(3), pp. 234–252.
[36] Carlson, J., and Doyle, J., 2000, "Highly Optimized Tolerance: Robustness and Design in Complex Systems," Phys. Rev. Lett., **84**(11), pp. 2529–2532.
[37] Nahm, Y., and Ishikawa, H., 2005, "Representing and Aggregating Engineering Quantities with Preference Structure for Set-Based Concurrent Engineering," Concurrent Eng. Res. Appl., **13**(2), pp. 123–133.
[38] Gventer, G., and Haftka, R., 1999, "Using Response Surface Methodology in Fuzzy Set Based Design Optimization," Struct. Optim., **18**(4), pp. 1–12.
[39] Kizer, J., and Mavris, D., 2014, "Set-Based Design Space Exploration Enabled by Dynamic Constraint Analysis," 29th Congress of the International Council of the Aeronautical Sciences (ICAS), St. Petersburg, Russia, Sept. 7–12.
[40] Shahan, D., and Seepersad, C., 2012, "Bayesian Network Classifiers for Set-Based Collaborative Design," ASME J. Mech. Des., **134**(7), p. 071001.
[41] Backlund, P., Shahan, D., and Seepersad, C., 2015, "Classifier-Guided Sampling for Discrete Variable, Discontinuous Design Space Exploration: Convergence and Computational Performance," Eng. Optim., **47**(5), pp. 579–600.
[42] Rosen, D., 2015, "A Set-Based Design Method for Material-Geometry Structures by Design Space Mapping," 2015 International Design Engineering Technical Conferences and Computers and Information in Engineering Conference, Boston, MA, Aug. 2–5, pp. 1–11.
[43] Landahl, J., Levandowski, C., Johannesson, H., and Isaksson, O., 2016, *Assessing Producibility of Product Platforms Using Set-Based Concurrent Engineering*, Vol. 4, IOS Press, Amsterdam, pp. 35–44.
[44] Wang, J., and Terpenny, J., 2003, "Interactive Evolutionary Solution Synthesis in Fuzzy Set-Based Preliminary Engineering Design," J. Intell. Manuf., **14**(2), pp. 153–167.
[45] Doerry, N., Earnesty, M., Weaver, C., Banko, J., Myers, J., Browne, D., Hopkins, M., and Balestrini, S., 2014, "Using Set-Based Design in Concept Exploration," NAME Chesapeake Section Technical Meeting, Army Navy Country Club, **1**(5), pp. 1–8.
[46] Malak, R., Aughenbaugh, J., and Paredis, C., 2009, "Multi-Attribute Utility Analysis in Set-Based Conceptual Design," CAD Comput. Aided Design, **41**(3), pp. 214–227.
[47] Avigad, G., and Moshaiov, A., 2009, "Set-Based Concept Selection in Multi-objective Problems: Optimality Versus Variability Approach," J. Eng. Design, **20**(3), pp. 217–242.
[48] Miller, S. W., Yukish, M. A., and Simpson, T. W., 2018, "Design As a Sequential Decision Process: A Method for Reducing Design Set Space Using Models to Bound Objectives," Struct. Multidiscipl. Optim., **57**(1), pp. 305–324.
[49] Hannapel, S., and Vlahopoulos, N., 2014, "Implementation of Set-Based Design in Multidisciplinary Design Optimization," Struct. Multidiscipl. Optim., **50**(1), pp. 101–112.
[50] Athan, T., and Papalambros, P., 1996, "A Note on Weighted Criteria Methods for Compromise Solutions in Multi-Objective Optimization," Eng. Optim., **27**(2), pp. 155–176.
[51] Ge, P., Lu, S., and Bukkapatnam, S., 2005, "Supporting Negotiations in the Early Stage of Large-Scale Mechanical System Design," ASME J. Mech. Des., **127**(6), pp. 1056–1067.
[52] Taguchi, G., 1987, *System of Experimental Design: Engineering Methods to Optimize Quality and Minimize Cost*, UNIPUB/Kraus International Publications, White Plains.
[53] Talgorn, B., Audet, C., Le Digabel, S., and Kokkolaras, M., 2018, "Locally Weighted Regression Models for Surrogate-Assisted Design Optimization," Optim. Eng., **19**(1), pp. 213–238.
[54] Lophaven, S., Nielsen, H., and Søndergaard, J., 2002, *DACE—A Matlab Kriging Toolbox, Version 2.0*.
[55] Audet, C., Kokkolaras, M., Le Digabel, S., and Talgorn, B., 2018, "Order-Based Error for Managing Ensembles of Surrogates in Mesh Adaptive Direct Search," J. Global Optim., **70**(3), pp. 645–675.
[56] Sobieszczanski-Sobieski, J., Barthelemyy, J.-F., and Riley, K., 1982, "Sensitivity of Optimum Solutions to Problem Parameters," AIAA J., **20**(9), pp. 1291–1299.
[57] McKay, M., Beckman, R., and Conover, W., 1979, "A Comparison of Three Methods for Selecting Values of Input Variables in the Analysis of Output From a Computer Code," Technometrics, **21**(2), pp. 239–245.
[58] Loeppky, J., Sacks, J., Welch, W., and Welch, W., 2008, Choosing the Sample Size of a Computer Experiment: A Practical Guide. Technical Report, National Institute of Statistical Sciences.
[59] Mukherjee, T., Zhang, W., and DebRoy, T., 2017, "An Improved Prediction of Residual Stresses and Distortion in Additive Manufacturing," Comput. Mater. Sci., **126**, pp. 360–372.
[60] Manvatkar, V. D., Gokhale, A. A., Jagan Reddy, G., Venkataramana, A., and De, A., 2011, "Estimation of Melt Pool Dimensions, Thermal Cycle, and Hardness Distribution in the Laser-Engineered Net Shaping Process of Austenitic Stainless Steel," Metall. Mater. Trans. A., **42**(13), pp. 4080–4087.
[61] Rosenthal, D., 1946, *The Theory of Moving Sources of Heat and its Application to Metal Treatments*, ASME, Cambridge.
[62] Goldak, J., Chakravarti, A., and Bibby, M., 1984, "A New Finite Element Model for Welding Heat Sources," Metallur. Trans. B, **15**(2), pp. 299–305.
[63] Nickel, A. H., Barnett, D. M., and Prinz, F. B., 2001, "Thermal Stresses and Deposition Patterns in Layered Manufacturing," Mater. Sci. Eng. A., **317**(1–2), pp. 59–64.
[64] Budynas, R. G., Nisbett, J. K., and Shigley, J. E., 2015, *Shigley's Mechanical Engineering Design*, 10th ed., McGraw-Hill Education, New York.
[65] Le Digabel, S., 2011, "Algorithm 909," ACM Trans. Math. Software, **37**(4), pp. 1–15.
[66] Audet, C., and Dennis, J. E., 2006, "Mesh Adaptive Direct Search Algorithms for Constrained Optimization," SIAM J. Optim., **17**(1), pp. 188–217.
[67] Barber, C., Dobkin, D., and Huhdanpaa, H., 2002, "The Quickhull Algorithm for Convex Hulls," ACM Trans. Math. Software, **22**(4), pp. 469–483.
[68] Brown, N., and Mueller, C., 2019, "Quantifying Diversity in Parametric Design: A Comparison of Possible Metrics," Artificial Intell. Eng. Design, Analysis Manufact., **33**(1), pp. 40–53.